1

2

Regulation of apical constriction via microtubule-dependent Fog signaling activity and apical enrichment of apical/junctional proteins during tissue invagination

6

7

8

9   Thao Phuong Le[1] and SeYeon Chung[1, *]

10   [1] Department of Biological Sciences, Louisiana State University, Baton Rouge, LA 70803, USA

12   [*]Author for correspondence: seyeonchung@lsu.edu

13

Abstract

The formation of an epithelial tube is a fundamental process for organogenesis. During *Drosophila* embryonic salivary gland (SG) invagination, Folded gastrulation (Fog)-dependent Rho-associated kinase (Rok) promotes contractile apical myosin formation to drive apical constriction. Microtubules (MTs) are also crucial for this process and are required for forming and maintaining apicomedial myosin. However, the underlying mechanism that coordinates actomyosin and MTs networks is still unclear. Here, we show that MT-dependent intracellular trafficking has regulates apical constriction during SG invagination. Key components involved in protein trafficking, such as Rab11 and Nuclear fallout (Nuf), are apically enriched near the SG invagination pit in a MT-dependent manner. Disruption of the MT networks or intracellular trafficking impairs apicomedial myosin formation and apical constriction. We show that MTs and dynein motors regulate Fog signaling activity. We further show that MTs are required for apical enrichment of key apical and junctional proteins in the SG, including the apical determinant protein Crumbs (Crb), the key adherens junction protein E-Cadherin (E-Cad) and the scaffolding protein Bazooka/Par3. Targeted knockdown of these genes in the SG disrupts apical myosin networks and results in apical constriction defects. Our data suggests a role of MT-dependent intracellular trafficking in regulating actomyosin networks and cell junctions, to coordinate cell behaviors during tubular organ formation.

Introduction

Formation of three-dimensional tubes by invagination of flat epithelial sheets is a fundamental process in forming organs such as the lungs and kidneys (Andrew and Ewald, 2010). To enter the third dimension, cells must change their shapes and positions relative to each other. A major cellular process during epithelial tube formation is apical constriction, a universal cell shape change that is linked to tissue bending, folding and invagination (Martin and Goldstein, 2014; Sawyer et al., 2010). During apical constriction, the apical side of an epithelial cell constricts, causing a columnar or cuboidal cell to become wedge-shaped (Martin and Goldstein, 2014; Sawyer et al., 2010). Manipulation of apical constriction in a group of cells impacts both local and global tissue shape directly, suggesting a critical role for apical constriction in forming proper tissue architecture (Chung et al., 2017; Guglielmi et al., 2015; Izquierdo et al., 2018).

Apical constriction is driven by actin filament (F-actin) networks and the molecular motor non-muscle myosin II (hereafter referred to as myosin). Over the past decade, important functions of different actomyosin structures in epithelial tissue morphogenesis have been discovered. Particularly, studies in *Drosophila* revealed a distinct population of pulsatile apical medial actomyosin (hereafter referred to as apicomedial myosin) that generates a pulling force that exerts on adherens junctions to drive apical constriction (Booth et al., 2014; Chung et al., 2017; Martin et al., 2009; Rauzi et al., 2010). In early *Drosophila* embryos, apicomedial myosin is created in response to signaling by the Folded gastrulation (Fog) ligand and its G protein-coupled receptors (GPCRs) (Kerridge et al., 2016; Manning et al., 2013), and is regulated by apical Rho-associated kinase (Rok) (Mason et al., 2013). Apical junctions and apical determinants also have an important role in the formation of functional actomyosin complexes. During *Drosophila* dorsal closure, the apical polarity regulators Par-6, aPKC and Bazooka/Par3 (Baz/Par3) (altogether known as the Par complex) regulate pulsed actomyosin contractions in amnioserosa cells (David et al., 2010). In the *Drosophila* embryonic trachea, the apical protein Crumbs (Crb) is required for proper organization of the actomyosin complex (Letizia et al., 2011).

Emerging evidence suggests that microtubules (MTs) play a critical role in tissue invagination (Booth et al., 2014; Ko et al., 2019). MTs serve as tracks in intracellular transport, raising the possibility that MTs regulate apical constriction through the endo- and exocytosis of membrane receptors and adhesion molecules (Khanal et al., 2016; Le Droguen et al., 2015). Several lines of evidence suggest the importance of the endocytic pathway, including the molecular motor dynamin and the vesicle trafficking Rab proteins, in apical constriction in both in vitro and in vivo systems. During *Xenopus* gastrulation, disrupting endocytosis with dominant-negative dynamin or Rab5 perturbs apical constriction and invagination of cell sheets (Lee and Harland, 2010). During *Drosophila* gastrulation, the apical surface of cells is reshaped via Rab35 and RabGEF Sbf, which direct the plasma membrane to Rab11-positive recycling endosomes through a dynamic interaction with Rab5 endosomes to reshape actomyosin networks (Miao et al., 2019). Moreover, in the developing neural tube in *Xenopus*, asymmetric enrichment of Rab11 at the medial apical junctions is critical for apical constriction, suggesting that membrane trafficking has a key role in apical constriction (Ossipova et al., 2014). However, exactly how membrane trafficking, MTs, and actomyosin networks are linked remains to be discovered.

To determine how these three cellular attributes contribute to tissue invagination, we use the *Drosophila* embryonic salivary gland (SG) as a model. We and others showed that apical constriction is regulated in a highly coordinated and spatiotemporally controlled manner during epithelial tube formation (Booth et al., 2014; Chung et al., 2017; Myat and Andrew, 2000; Sanchez-Corrales et al., 2018). The *Drosophila* embryo forms two SG tubes via invagination of two epithelial placodes on the ventral surface (Chung et al., 2014). Before invagination, a small group of cells in the dorsal/posterior region of each SG placode begin to constrict. As those cells internalize to form the invagination pit, more cells anterior to the pit undergo clustered apical constriction in a Fog signaling-dependent manner (Chung et al., 2017) (Figure 1A). In the absence of *fog*, SG cells fail to accumulate Rok and myosin in the apicomedial region of the cells. MTs aid in the formation and maintenance of the apicomedial myosin network during SG invagination (Booth et al., 2014). The MT cytoskeleton near the invagination pit forms a network of longitudinal MT bundles, with the minus ends of MTs facing the apical domain of the cells and interacting

93   with the apicomedial myosin (Booth et al., 2014). Disruption of MTs causes loss of

94   apicomedial myosin and disrupted apical constriction during SG invagination (Booth et

95   al., 2014). However, it is still unknown how intracellular trafficking affects these two

96   processes.

97   In this study, we demonstrate that key proteins involved in intracellular trafficking -

98   including Rab11, its binding partner Nuclear fallout (Nuf), and dynein heavy chain - are

99   enriched in the apical domain of SG cells during invagination. Moreover, this

100 accumulation is MT-dependent. Our data suggest that apical enrichment of several

101 proteins, including the apical determinant protein Crb, the key adherens junction protein

102 E-Cadherin (E-Cad), and the scaffolding protein Baz/Par3, is compromised when the MT

103 networks are disrupted. We further show that disruption of MTs or reducing dynein heavy

104 chain leads to a decrease of Rok and myosin in the apical domain and causes

105 uncoordinated apical constriction in the SG. Altogether, our work mechanistically links

106 MT-dependent intracellular trafficking to the regulation of actomyosin networks during

107 tubular organ formation.

108

109 **Results**

110 **Intracellular trafficking components are apically enriched near the invagination pit**

111 To test a role for the intracellular trafficking machinery in spatially biased signaling

112 activation and protein accumulation during SG invagination, we analyzed the subcellular

113 localization of proteins that are involved in vesicle trafficking in the SG. Several endosome

114 markers were tested, including Rab5 (an early endosome marker) (Gorvel et al., 1991),

115 Rab7 (a late endosome marker) (Meresse et al., 1995; Wichmann et al., 1992), Rab11 (a

116 recycling endosome marker) (Ullrich et al., 1996), Nuclear fallout (Nuf, a putative binding

117 partner for Rab11) (Riggs et al., 2003), and Sec15 (an exocyst complex component and

118 effector for Rab11) (Langevin et al., 2005; Zhang et al., 2004). We observed enrichment

119 of Rab11, Nuf, and Sec15 at and near the SG invagination pit, suggesting active

120 trafficking activities in the region where cells are apically constricting (Figure 1C-1D', 1G-

121   1H'; Figure S1A-S1C). Compared to a more uniform distribution of Rab11 and Nuf in the

122   entire apical domain, Sec15 signals appeared to be enriched at adherens junctions

123   (Figure S1B). Using labeling with E-Cad, an adherens junction marker, and CrebA, a SG

124   nuclear marker, we segmented apical cell outlines (Figure 1B and 1B'). Intensity mean of

125   Rab11 or Nuf in the apical domain of each cell showed a negative correlation with the

126   apical area of cells in the entire SG (Figure 1E), further supporting the conclusion that

127   increased trafficking and apical constriction are closely linked.

128   Rab5, an early endosome marker, was also upregulated near the invagination pit,

129   suggesting active endocytosis in this region (Figure S1B and S1B'). Dynein heavy chain

130   64C, a subunit of the dynein motor complex that transports cargos along MTs toward their

131   minus ends, also showed upregulation near the invagination pit (Figure 1J and 1J'). Rab7,

132   a late endosome marker, however, did not show any enrichment but localized as large

133   punctate structures in the cytoplasm of the entire SG placode (Figure 1L and 1L'),

134   suggesting that trafficking from early to late endosomes or between late endosomes to

135   lysosomes is not upregulated near the pit during SG invagination. Overall, our results

136   suggest active intracellular trafficking, possibly both endo- and exocytosis, near the

137   invagination pit during SG invagination.

138

139   **MT-dependent vesicular transport is required for apical constriction in the SG**

140   Strong apical enrichment of Rab11 and Nuf in the SG cells near the invagination pit led

141   us to test whether these vesicle markers are associated with vertically aligned MTs that

142   could facilitate their polarized distribution. As in many epithelial cells, MT minus- and plus-

143   ends face the apical and the basal domain of the SG cells, respectively (Booth et al.,

144   2014; Myat and Andrew, 2002). Indeed, co-immunostaining of tyrosinated α-tubulin, a

145   marker of dynamic or newly polymerized MTs, and Rab11 showed a partial overlap of the

146   two proteins at the apical region of the SG cells (Figure 2A'-2B''). Mander's overlap

147   coefficients of Rab11 and tyrosinated α-tubulin revealed that 59% of Rab11 signals

148   overlapped with tyrosinated α-tubulin labeling and 34% of tyrosinated α-tubulin signals

149   co-localized with Rab11 signals (Figure 2C).

6

150　　To test whether Rab11 apical enrichment in SG cells is dependent on MT networks, we

151　　disrupted MTs in the SG by overexpressing spastin, a MT-severing protein (Sherwood et

152　　al., 2004), using the SG-specific *fkh-Gal4* driver. In control SGs, tyrosinated α-tubulin and

153　　acetylated α-tubulin, a marker of stable and longer-lived MTs (Westermann and Weber,

154　　2003), were observed abundantly in the apical domain of cells in the whole placode

155　　(Figure 2D'' and 2D'''; Figure S2). In spastin-overexpressing SGs, both tyrosinated and

156　　acetylated α-tubulin signals were strongly reduced, revealing loss of MT filaments (Booth

157　　et al., 2014) (Figure 2E'', 2E''' and S2B''); the upregulation of Rab11 near the invagination

158　　pit (Figure 2D') was also abolished and Rab11 was mislocalized basolaterally (Figure 2E'

159　　and 2F'). Quantification of Rab11 localization showed that SGs with disrupted MTs

160　　showed much lower intensity in the apical domain near the invagination pit compared to

161　　control SGs (Figure 1C' versus Figure 2G'). Similar patterns were observed for Nuf

162　　(Figure 2F-2H). These data suggest that MT networks are required for apical enrichment

163　　of Rab11 and Nuf during SG invagination.

164　　We next asked if specific modulation of Rab11 levels could compromise apical

165　　constriction. To test this possibility, we disrupted the function of Rab11 by overexpressing

166　　a dominant-negative form of Rab11 (Rab11S25N-YFP; hereafter referred to as Rab11-

167　　DN) in the SG. Compared to controls (Figure 3A), SGs overexpressing Rab11-DN

168　　showed more cells with larger apical area (Figure 3B and 3F), suggesting a role for Rab11

169　　in apical constriction during SG invagination.

170　　As dynein heavy chain was also enriched near the invagination pit (Figure 1J and 1J''),

171　　we hypothesized that dynein motors may traffic key proteins along MTs to control apical

172　　constriction during SG invagination. Indeed, zygotic knockdown of *Dynein heavy chain*

173　　*64C* (*Dhc64C*) in the SG resulted in more cells with larger apical areas during

174　　invagination, suggesting defective apical constriction (Figure 3C, 3C' and 3F). Since

175　　*Dhc64C* has strong maternal expression and is essential for oogenesis and early embryo

176　　development (Li et al., 1994), we tried to reduce Dhc64C levels still further by knocking

177　　down *Dhc64C* both maternally and zygotically, using a maternal driver *matα-Gal4* along

178　　with the SG-specific *fkh-Gal4*. Embryos with reduced maternal and zygotic pools of

179　　Dhc64C showed a range of morphological defects in the entire embryo, some of which

180 were severely distorted (data not shown). In embryos with more subtle morphological

181 defects, SG cells still invaginated and formed a tube. However, SGs showed a range of

182 phenotypes, from relatively normal but with slightly larger apical areas in individual cells

183 (Figure 3G; mild), to an enlarged invagination pit (Figure 3G; intermediate), to quite

184 distorted (Figure 3G; severe).

185 Klarsicht (Klar), the *Drosophila* Klarsicht-Anc-Syne Homology (KASH) domain protein,

186 mediates apical transport in the SG (Myat and Andrew, 2002) via the MT motor

187 cytoplasmic dynein (Gross et al., 2000). We therefore predicted that *klar* would also

188 influence apical constriction during SG invagination. Indeed, *klar* mutant embryos showed

189 SGs with mild apical constriction defects compared to wild type controls (Figure 3D-3E'

190 and 3F). Overall, our data suggest essential roles of Rab11 trafficking and MT- and

191 dynein-dependent transport in regulating apical constriction during SG invagination.

192

193 **Reduced dynein motor activity leads to failure in accumulation of apicomedial Rok**

194 **and reduction of apicomedial myosin formation in SG cells**

195 The apicomedial myosin structure generates the pulling force to drive apical constriction

196 in SG cells (Booth et al., 2014; Chung et al., 2017), and spastin overexpression inhibits

197 formation of apicomedial myosin during SG invagination (Booth et al., 2014). We

198 therefore tested whether apicomedial myosin formation is affected in SG cells when

199 dynein-dependent transport is compromised. In control SGs, sqh-GFP (a functional GFP-

200 tagged version of the myosin regulatory light chain) (Royou et al., 2004) showed a strong

201 apicomedial myosin web in constricting cells near the invagination pit (Figure 4A-4A'''').

202 Knockdown of *Dhc64C* caused a significant reduction of apicomedial myosin (Figure 4B-

203 4B'''' and 4C), suggesting its role in forming and/or maintaining apicomedial myosin.

204 Consistent with previous studies (Chung et al., 2017; Roper, 2012), a myosin pool that is

205 closely associated with adherens junctions, junctional myosin, also showed strong signals

206 in wild type SG cells, often with stronger signals at vertices (Figure 4A-4A'''). Intriguingly,

207 the intensity of junctional myosin was also reduced upon *Dhc64C* knockdown (Figure 4B-

8

208 4B''' and 4C). The ratio of apicomedial to junctional myosin was significantly reduced in

209 *Dhc64C* RNAi SGs (Figure 4C), suggesting a more significant effect on apicomedial than

210 on junctional myosin upon *Dhc64C* knockdown. Similar to *Dhc64C* knockdown, reduction

211 of apicomedial and junctional myosin was observed in *klar* mutant SGs (Figure 4D-4F).

212 Our data suggests that defective apical constriction in *Dhc64C* RNAi and *klar* mutant SGs

213 could be due to failure in proper organization of myosin structures, primarily in the

214 apicomedial region of SG cells.

215 We previously showed that Fog signaling-dependent accumulation of apical medial Rok

216 is required for apicomedial myosin formation for coordinated apical constriction in SG

217 cells (Chung et al., 2017). To test whether Rok accumulation is dependent on MTs, we

218 quantitatively analyzed Rok distribution using a ubiquitously expressed GFP-tagged Rok

219 transgene (Rok-GFP) (Abreu-Blanco et al., 2014) in wild type and MT-disrupted SGs.

220 Disruption of MTs by overexpression of spastin abolished the apicomedial accumulation

221 of Rok in cells near the invagination pit, found in control SGs (Figure 5A-5B'' and 5G).

222 We also tested for accumulation of apicomedial Rok-GFP signals in *Dhc64C* RNAi and

223 *klar* mutant SGs. Similar to spastin overexpression, reduction of *Dhc64C* levels led to

224 more dispersed Rok signals along the apical domain of SG cells near the pit (Figure 5C-

225 5C'' and 5G). In *klar* mutants, Rok-GFP tended to accumulate less profoundly and less

226 uniformly in the apicomedial region of SG cells (Figure 5E-5E'') although not statistically

227 significant compared to control (Figure 5H). Overall, our data suggest that MT- and

228 dynein-dependent apical accumulation of Rok and apicomedial myosin formation during

229 SG invagination.

230

231 **Fog signaling activity is reduced when MTs are disrupted**

232 Since Rok accumulation, apicomedial myosin formation, and subsequent coordinated

233 apical constriction in the SG are Fog-dependent (Chung et al., 2017), we tested whether

234 the roles of Fog signaling and MT trafficking in apical constriction were dependent on

235 each other. Although the existing Fog antibody (Fuse et al., 2013) detected the

236   endogenous Fog protein in the SG lumen at later stages, the signals at stage 11 were not

237   strong enough to show precise subcellular localization of Fog in the SG. We therefore

238   overexpressed Fog in the SG to saturate the transport system and test a role of MTs in

239   transporting Fog in this sensitized background. Consistent with our previous data that Fog

240   signal mediates apicomedial Rok accumulation and apicomedial myosin formation

241   (Chung et al., 2017), Fog-overexpressing SG cells over-accumulated Rok in the

242   apicomedial region and dramatically increased apicomedial myosin (Figure 6B and 6B').

243   This Fog gain-of-function effect on over-accumulation of Rok and increased apicomedial

244   myosin was suppressed by spastin overexpression or *Dhc64C* knockdown (Figure 6C-

245   6D', 6G-6H', 6J and 6L). Interestingly, we also observed highly ruffled SG cell junctional

246   morphology in almost all SG cells when Fog was overexpressed (Figure 6I and 6I').

247   Similar cell distortions, albeit in a moderate level, have been observed during apical

248   constriction in mesodermal cells (Martin et al., 2009) and in SG cells (Chung et al., 2017)

249   when apicomedial myosin exerts the pulling force on adherens junctions. Indeed,

250   increased apicomedial myosin was connected with E-Cad signals at distorted cell

251   junctions (Figure 6I and 6I'), suggesting that this ruffled junctional phenotype is due to

252   increased pulling forces generated by high levels of apicomedial myosin upon increased

253   Fog signaling activity. This convoluted junctional phenotype was suppressed by spastin

254   overexpression or *Dhc64C* knockdown (Figure 6G-6H' and 6K). Taken together, our data

255   suggest that MTs and dynein motors are necessary for Fog signaling activity and its

256   downstream targets Rok and myosin.

257

Enrichment of key apical and junctional proteins is MT-dependent and is required
258

for apical constriction during SG invagination
259

260   Transport of several key apical and junctional proteins is dependent on MTs and Rab11

261   (Jouette et al., 2019; Khanal et al., 2016; Le Droguen et al., 2015). One such protein is

262   an apical transmembrane protein Crb, and Rab11 helps maintain apical Crb in the

263   *Drosophila* ectoderm (Roeth et al., 2009). In the *Drosophila* SG and follicle cells, Crb is

264   apically transported along MTs by the dynein motor (Myat and Andrew, 2002) (Aguilar-

10

265 Aragon et al., 2019). Importantly, in *Drosophila* tracheae, loss of *crb* impairs apical

266 constriction during the internalization process (Letizia et al., 2011). Two key junctional

267 proteins, E-Cad and Baz/Par3, are also trafficked by MTs in *Drosophila* embryonic

268 trachea (Le Droguen et al., 2015). During apical constriction, contractile forces generated

269 by the actomyosin complex are exerted on adherens junctions, with E-Cad being a core

270 component that integrates contractile forces to generate tension (Martin et al., 2009).

271 During amnioserosa apical constriction at *Drosophila* dorsal closure, Baz/Par3 in the Par

272 complex regulates pulsed actomyosin contractions (David et al., 2010).

273 We therefore asked if MTs have a role in apical enrichment of Crb, E-Cad and Baz in the

274 SG during invagination. Consistent with previous studies (Myat and Andrew, 2002; Roper,

275 2012), Crb was upregulated near the invagination pit during SG invagination (Figure 7A).

276 E-Cad and Baz were also upregulated near the invagination pit (Figure 7A' and 7E).

277 Disruption of MTs resulted in reduction of Crb, E-Cad and Baz signals compared to control

278 (Figure 7A-7B'' and 7E-7I). Moreover, spastin overexpression caused discontinuous Crb

279 signals along the junctions (Figure 7D). Whereas the number of gaps was not significantly

280 different between control and spastin-overexpressing SGs (Figure 7K), quantification of

281 the ratio of length of gaps to junctional length revealed increased gap length in spastin-

282 overexpressing SGs (Figure 7J). These data suggest that apical enrichment of Crb, E-

283 Cad and Baz in the SG is dependent on MTs.

284 We further tested MT-dependent apical transport of Crb in the SG using the same genetic

285 suppression strategy as we used for testing a role of MTs in Fog trafficking (Figure 6C-

286 6C'). We co-overexpressed Crb and spastin in the SG to test whether disruption of MTs

287 affects apical transport of Crb. A similar approach was taken in a recent study, where

288 overexpression of Crb provided a highly sensitive genetic background for identifying

289 components involved in Crb trafficking (Aguilar-Aragon et al., 2019). Consistent with

290 previous findings that Crb expression expands apical membranes in epithelial cells

291 (Chung and Andrew, 2014; Chung et al., 2017; Myat and Andrew, 2002; Wodarz et al.,

292 1993), overexpression of Crb resulted in enlarged apical areas of SG cells during

293 invagination (Figure S3B-S3B'). Unlike control SG cells, Crb-overexpressing SG cells

294 also showed over-accumulation of Crb on the apical surface (Figure S3A-S3B'). Co-

295   overexpression of spastin and Crb suppressed this accumulation of Crb (Figure S3C and

296   S3C'), further supporting the idea that apical transport of Crb in the SG is dependent on

297   MTs.

298   To test for a role of Crb, E-Cad and Baz in regulating apical constriction during SG

299   invagination, we knocked down each gene in the SG using RNAi. Knockdown of *crb, E-*

300   *Cad* or *baz* resulted in reduction of junctional Crb, E-Cad or Baz levels, respectively,

301   compared to control (Figure S4A-S4C''). Reduction of *crb, E-Cad* or baz increased the

302   number of cells that have larger apical areas compared to control (Figure 7L-7N').

303   Quantification of the percentage of cells and cumulative percentage of cells of different

304   apical areas showed a significant decrease in the number of constricting cells in *crb* and

305   *baz* knockdown SGs (Figure 7O). *E-Cad* knockdown SGs also displayed a similar trend

306   although with less statistical significance (Figure 7O). Overall, our data suggest a role of

307   Crb, E-Cad and Baz in regulating apical constriction during SG invagination.

308

309   Apical localization of Crb, E-Cad and Baz is MT- and Rab11-dependent in the SG

310   throughout development

311   To further investigate the role of MTs in apical trafficking of Crb, E-Cad and Baz in the

312   SG, we overexpressed spastin throughout development and analyzed late stage SGs,

313   where apical trafficking is more easily detected in elongated SG cells. Analysis of spastin-

314   overexpressing SGs at stage 16 revealed that disruption of MTs resulted in short SG

315   tubes with a thin lumen compared to control SGs of the same stage (Figure S5A and

316   S5B). Strikingly, whereas the majority of Rab11- and Nuf-positive vesicles localized in the

317   apical region of control SG cells (Figure S5A-S5A'''), Rab11 and Nuf were observed as

318   large aggregates in the cytoplasm in spastin-overexpressing cells, overlapping with each

319   other (Figure S5B-S5B'''). Our data suggest that MTs are required for apical enrichment

320   of Rab11/Nuf vesicles throughout SG tube formation.

321   Using the same co-overexpression strategy that we used for stage 11 (Figure S3B-S3C'),

322   we tested whether MTs and Rab11 are required for apical trafficking of Crb, E-Cad and

12

323   Baz also at stage 16. Consistent with previous studies (Chung and Andrew, 2014; Wodarz

324   et al., 1993), Crb overexpression in the SG caused a dramatic increase of the apical

325   membrane as well as mislocalization of Crb basolaterally along the entire membrane

326   (Figure S5C-S5C'''). Overexpression of E-Cad alone using UAS-Shotgun-GFP (Shg,

327   *Drosophila* E-Cad; Rorth, 2014) did not result in overt morphological defects in the SG,

328   and punctate E-Cad signals mostly overlapped with Nuf signals at and near adherens

329   junctions (Figure S5E-S5E'''). Overexpression of Baz using UAS-Baz-GFP (Benton and

330   St Johnston, 2003) in the SG caused a slightly enlarged lumen (Figure S5G-S5G'''). Baz-

331   GFP signals were detected mostly at adherens junctions, but small punctate structures

332   were also detected in the cytoplasm (Figure S5G').

333   Co-overexpression of spastin along with Crb or Baz suppressed the overexpression

334   phenotypes for Crb or Baz (Figure S5D-S5D''' and S5H-S5H''). Importantly, in SGs that

335   co-overexpressed spastin along with any of these three apical/junctional proteins, each

336   protein mislocalized as cytoplasmic aggregates near the basolateral domain, which were

337   largely overlapping with mislocalized Rab11/Nuf (Figure S5D-S5D''', S5F-S5F''' and S5H-

338   S5H'''). Overall, our data suggest that several key proteins, including Crb, E-Cad and Baz,

339   are trafficked apically in a MT- and Rab11-dependent manner in the SG throughout tube

340   formation.

341

342   **Reducing apical and junctional proteins affects Rok accumulation and apicomedial**

343   **myosin formation**

344   To test whether apical constriction defects observed in *crb*, *E-Cad* and *baz* knockdown

345   SGs (Figure 7L-7O) are linked to apicomedial myosin formation, we analyzed myosin

346   levels in SGs with these knockdowns. Overall myosin levels were reduced in *crb* or *baz*

347   knockdown SGs, both in the apicomedial region and at adherens junctions (Figure 8A-

348   7A'', 8B-8B'', 8D-8D'' and 8E). The ratio of apicomedial to junctional myosin was also

349   reduced (Figure 8E), suggesting that apical constriction defects in SGs depleted of *crb* or

350   *baz* are, at least in part, due to failure of apicomedial myosin formation. In SGs depleted

351   of *E-Cad*, myosin levels at each domain did not change significantly, but the ratio of

352   apicomedial myosin to junctional myosin was significantly reduced compared to control

353   (Figure 8C-8C'' and 8E). Therefore, the apical constriction defects caused by *E-Cad*

354   knockdown might be due to an imbalance of contractile forces.

355   Knockdown of *crb* or *baz* also resulted in Rok-GFP signals less accumulating in the apical

356   region of cells near the invagination pit (Figure 8G-8I''). Quantification of the areas

357   occupied by Rok-GFP puncta showed significant reduction in accumulation of

358   apicomedial Rok when *crb* or *baz* was knocked down (Figure 8J). Consistent with the

359   relatively mild effect of *E-Cad* knockdown on apicomedial myosin (Figure 8C-8C'' and

360   8E), Rok accumulation was not significantly affected by *E-Cad* knockdown. Several SG

361   cells, however, showed dispersed Rok-GFP signals in cells near the invagination pit,

362   which was not observed in control cells (Figure 8H-8H'' and 8J), suggesting some defects

363   in Rok accumulation. Taken together, our results suggest a role for Crb and Baz in

364   regulating apical constriction by mediating Rok accumulation and myosin activation

365   during SG invagination.

366

367   **Discussion**

368   **MT-dependent intracellular trafficking during apical constriction**

369   Using the *Drosophila* SG, we demonstrate that MT-dependent intracellular trafficking is

370   critical for apical constriction during tissue invagination. MTs have been shown to have a

371   crucial role in stabilizing apical myosin during epithelial morphogenesis both in early

372   *Drosophila* embryos and in the *Drosophila* SG (Booth et al., 2014; Ko et al., 2019).

373   Particularly in the SG, MTs interact with apicomedial myosin via Short stop, the

374   *Drosophila* spectraplakin, emphasizing a direct interplay between the MT and the apical

375   myosin networks (Booth et al., 2014). Our data reveals another role of MTs in regulating

376   protein trafficking to control the apical myosin networks during tissue invagination. During

377   SG invagination, a network of longitudinal MT bundles is observed near the invagination

378   pit (Booth et al., 2014). Our data shows apical enrichment of key endocytic markers in the

379   same area and that this enrichment is important for forming the apicomedial myosin

380 networks (Figure 1-4), suggesting a link between localized protein trafficking along MTs
381 to apical myosin regulation. Our data support a model that dynein- and Rab11-dependent
382 intracellular trafficking is crucial for organizing apical myosin networks during apical
383 constriction in the SG.

384 Interestingly, cytoplasmic dynein is associated with cellular structures and exerts tension
385 on MTs. For example, dynein tethered at the cell cortex can apply a pulling force on the
386 MT network by walking towards the minus end of a MT (Laan et al., 2012). In interphase
387 cells, force generated by dynein also regulates MT turnover and organization (Yvon et
388 al., 2001). Therefore, we do not rule out the possibility that reduced dynein functions could
389 affect MT organization and/or a pulling force on the MT networks regardless of its role in
390 intracellular trafficking, which will subsequently affect apical myosin structures during SG
391 invagination. However, we favor the apical trafficking model as we did not observe overt
392 changes in the MT networks in *Dhc64C* RNAi SGs (data not shown).

393

394 **Integrating apical and junctional proteins with actomyosin networks during SG**
395 **invagination**

396 During branching morphogenesis in *Drosophila* trachea, MTs and dynein motors have a
397 critical role in proper localization of junctional proteins such as E-Cad and Baz (Le
398 Droguen et al., 2015). This is consistent with our observations with MT-dependent
399 trafficking of Crb, E-Cad and Baz in both early (Figure 7) and late stage SG (Figure S5),
400 suggesting a conserved role of MT-dependent intracellular trafficking in junctional
401 remodeling and stabilization during epithelial tube formation. Our data suggests that
402 proper levels of apical and junctional proteins are also important for tissue invagination at
403 the beginning of epithelial tube formation. Dispersed Rok and less prominent apicomedial
404 myosin are observed in invaginating SGs upon knockdown of *crb*, *E-Cad* and *baz* (Figure
405 8), suggest a requirement of apical and junctional proteins in proper organization of apical
406 actomyosin networks during epithelial tube formation. We propose that MTs and Rab11
407 play a role in apical trafficking of these proteins during SG invagination and throughout
408 SG tube formation. Alternatively, MTs have a role in assembling/anchoring these apical

15

409   components, through regulation of unidentified molecules. Recent studies in *Drosophila*
410   mesoderm invagination showed that MTs help to establish actomyosin network linked to
411   cell junction to facilitate efficient force transmission to promote apical constriction (Ko et
412   al., 2019). In Ko et al., (2019), however, MT-interfering drugs and RNAi of CAMSAP end-
413   binding protein were used to prevent MT functions and the effect cannot be directly
414   compared to our data where spastin was used to sever existing MTs. Further work will be
415   needed to directly monitor MT-dependent transport of Crb, E-Cad and Baz during SG
416   invagination and clarify the mechanism.

417   When *crb* is knocked down using RNAi in the SG, overall intensity of myosin is decreased
418   near the invagination pit, for both apicomedial and junctional pools (Figure 8). It is possible
419   that proper Crb levels are required for modulating myosin activity both in the apical
420   domain and at junctions, which contribute to apical constriction and cell rearrangement
421   during SG invagination. Anisotropic localization of Crb and myosin was observed at the
422   boundary of the SG placode, where myosin accumulates at edges where Crb is lowest
423   (Roper, 2012). Planar polarization of Rok at this boundary is modulated through
424   phosphorylation by Pak1 downstream of Crb (Sidor et al., 2020). It will be interesting to
425   further test how Crb might affect junctional myosin dynamics and SG invagination.

426   As contractile actomyosin structures exert forces on adherens junction to drive apical
427   constriction, we speculate that slight reduction of apicomedial myosin upon *E-Cad* RNAi
428   might be due to reduction of cell adhesion. Also, decrease of apicomedial and junctional
429   myosin caused by *baz* knockdown is consistent with the role of the Par complex in
430   regulating pulsed actomyosin contraction during *Drosophila* dorsal closure (David et al.,
431   2010). It will be interesting to determine if coordination of apical and junctional proteins
432   and apical cytoskeletal networks through intracellular trafficking is conserved during
433   tubular organ formation in general.

434

435   **Regulation of Fog signaling activity**

16

436   The Fog pathway represents one of the best-understood signaling cascades controlling
437   epithelial morphogenesis (Manning and Rogers, 2014). Although best studied in
438   *Drosophila*, the pathway components have been also identified in other insects,
439   suggesting a more widely conserved role of Fog signaling in development (Benton et al.,
440   2019; Urbansky et al., 2016). The dorsal/posterior region of the SG where Dhc64C is
441   apically enriched (Figure 1) correlates with localized Fog signaling activity that promotes
442   clustered apical constriction (Chung et al., 2017). Disruption of MTs or *Dhc64C*
443   knockdown not only causes dispersed Rok and defective apicomedial myosin (Figure 5),
444   which is reminiscent of *fog* mutant phenotypes, but also suppresses the Fog gain-of-
445   function effect on Rok and myosin (Figure 6). We propose that dynein-dependent apical
446   trafficking is important for regulating Fog signaling activity to control apical constriction
447   during epithelial tube formation. A possible scenario is that dynein-dependent apically
448   targeted vesicles contain key components of the Fog signaling pathway, such as the Fog
449   ligand and/or the as yet unidentified SG receptor(s) of Fog.

450   Apical enrichment of Rab11/Nuf is also MT-dependent during SG invagination and
451   disruption of the Rab11 function inhibits apical constriction in SGs (Figure 3). Unlike other
452   apical or junctional proteins that we have tested (Crb, E-Cad and Baz) that colocalize with
453   Rab11/Nuf when mislocalized, mislocalized Fog did not co-localize with Rab11 or Nuf
454   (Figure S6). It could be explained by the fact that Rab11 is primarily associated with
455   recycling endosomes; when Fog is not used, it is most likely degraded rather than
456   recycled. As recycling of membrane receptors to the cell surface plays an important role
457   in the regulation of overall signaling activity, it is possible that Rab11 is also involved in
458   recycling of the Fog receptor(s) to regulate Fog activity in the SG. Indeed, several GPCRs
459   are recycled via Rab11 (Anborgh et al., 2000; Cerniello et al., 2017; Dale et al., 2004; Fan
460   et al., 2003; Hamelin et al., 2005; Hunyady et al., 2002; Innamorati et al., 2001; Volpicelli
461   et al., 2002). Further work needs to be done to fully understand the mechanisms
462   underlying trafficking of Fog and its receptor(s) and how the signaling pathway is able to
463   generate cellular forces to drive cell shape changes during epithelial morphogenesis.

464

17

465 **Materials and Methods**

466 **Fly stocks and husbandry**

467 Fly lines used in our experiments were listed in a separate table. All crosses were
468 performed at 25°C, unless stated otherwise.

469

470 **Antibody staining and confocal microscopy**

471 Antibodies used in our experiments were listed in a separate table. Embryos were
472 collected on grape juice-agar plates and processed for immunofluorescence using
473 standard procedures. Briefly, embryos were dechorionated in 50% bleach, fixed in 1:1
474 heptane:formaldehyde for 40 min and devitellinized with 80% EtOH, then stained with
475 primary and secondary antibodies in PBSTB (1X PBS, 0.1% Triton X-100, 0.2% BSA).
476 For acetylated α-tubulin, tyrosinated α-tubulin staining, embryos were hand-devitellinized.
477 All images were taken with a Leica SP8 confocal microscope.

478

479 **Cell segmentation and apical area quantification**

480 Embryos immunostained with E-Cad and CrebA were imaged using a Leica SP8 confocal
481 microscope. Since Rok accumulation, apicomedial myosin and apical constriction depend
482 on the depth of invagination in the SG, SGs that were invaginated within the range of 5.1-
483 9.9 μm depth were used for quantification for proper comparison between different
484 genotypes. Maximum intensity projection was generated from three apical focal planes
485 with highest E-Cad signals for all genotypes, except for maternal/zygotic knockdown of
486 *Dhc64C*, where 10 to 30 focal planes were used due to wavy epithelial morphology (0.3
487 μm apart for each focal plane). Cells were segmented along the E-Cad signals and cell
488 areas were calculated using the Imaris Program (Bitplane). Since the Imaris Program
489 calculated the areas of both the front and the back of the projected cell layer, we divided
490 the measured areas by two to get the true values of apical areas of SG cells.

18

491

Negative correlation between apical area and Rab11/Nuf intensity

Cell segmentation for five WT SGs within the range of 5.1- 9.9 µm invagination was performed as described above. All experiments were carried out in the same condition and the same setting for confocal imaging was used. Intensity mean was measured for the entire Rab11/Nuf signals for each segmented cell using the Imaris Program (Bitplane) and plotted. Correlation (Pearson) and P values were calculated using the GraphPad Prism software.

To compare the enrichment of Rab11/Nuf near the invagination pit of the WT SG to the spastin overexpressed SG, the ratio of deviation of Rab11/Nuf intensity to median Rab11/Nuf intensity was used. Median value of Rab11/Nuf intensity is the average of Rab11/Nuf mean intensities in all SG cells. Deviation of Rab11/Nuf intensity is the difference between the mean intensity of each cell and the median value. Five WT SGs (690 cells) and four spastin-overexpressed SGs (396 cells) were analyzed and plotted. P values were calculated using the Mann-Whitney U test in the GraphPad Prism software.

506

Colocalization analysis

Colocalization analyses were performed with the JACOP plugin in Fiji software. Thresholded Manders' overlap coefficients were used to show the extent to which two proteins colocalize. Manders' coefficients, vary from 0 to 1, are indicators of overlap between two proteins and are independent of signal proportionality. The Manders' overlap coefficient for Rab11 is the proportional Rab11 that is colocalized with tyrosinated α-tubulin. The Manders' overlap coefficient for tyrosinated α-tubulin is the proportional tyrosinated α-tubulin that is colocalized with Rab11. For each SG, the dorsal/posterior region of 100 µm^2 where Rab11 is upregulated was tested. Six WT embryos were used for quantification.

517

19

Quantification of the intensity of myosin, Crb, E-Cad and Baz

518

519   A group of 30 (for control and spastin-overexpressing SGs in Figure 7) or 10 (for all other

520   genotypes) cells in the dorsal/posterior region of SG placode near the invagination pit

521   were selected for quantification. For myosin quantification, maximum intensity projections

522   that span the apical and the junctional region of SG cells were used (Leica LasX) and

523   measurements were performed using the Fiji software. Regions were drawn manually

524   along the inner or outer boundary of E-Cad signals of each cell to calculate the mean gray

525   value of apicomedial and junctional myosin. For background correction, mean gray values

526   of apicomedial myosin in ten cells outside of the SG placode was measured. The average

527   value of mean gray values of apicomedial myosin in these ten cells was used to subtract

528   the background of the cells inside the placode from the same embryo. For each genotype,

529   five SGs were used for quantification. P values were calculated using the Mann-Whitney

530   U test in the GraphPad Prism software. Mean gray values of Crb, E-Cad and Baz were

531   measured with the same method used for quantifying the mean gray value of junctional

532   myosin.

533

Quantification of area of Rok puncta

534

535   A single confocal section that had the strongest medial Rok signals was selected. Cell

536   boundaries were labeled by immunostaining with the antibody against E-Cad. To analyze

537   Rok distribution, we performed particles analysis using the Fiji software. 15 cells in the

538   dorsal/posterior region near the invagination pit were selected for quantification. Rok-GFP

539   signals were converted into black-and-white using the *Threshold* tool in Photoshop before

540   analysis. Using the *Analyze particles* tool in Fiji, Rok-GFP puncta with areas equal or

541   larger than 0.02 μm^2 were measured. Five SGs were used for quantification. P values

542   were calculated using the Mann-Whitney U test in the GraphPad Prism software.

543

Quantification of tortuosity

544

545   10 cells in the dorsal/posterior region near the invagination pit of the SG placode were

546   selected for quantification. Using the Fiji software, the actual length of a given adherens

547   junction (L) was calculated using the E-Cad signals. The tortuosity was calculated as the

548   ratio of the junctional length (L) and the shortest distance (L_o) between the two vertices

549   (tortuosity= L/L_o). Five SGs were used for quantification for each genotype. P values were

550   calculated using the Mann-Whitney U test in the GraphPad Prism software.

551

Quantification of length and number of gaps of junctional Crb

553   Length of gaps and junctional length were measured using the Fiji software. Gaps that

554   have the length equal or more than 0.2 μm were quantified. If there were more than one

555   gap per junction, the length of gaps was calculated as a sum of all gaps in a given junction.

556   For each SG, 10 cells in the dorsal/posterior region were used for quantification. For the

557   number of gaps, the total number of gaps in those 10 cells were counted. Four SGs (~90

558   junctions) were used for quantification.

559

Fly strains	Source	RRID	References
Rab11-EYFP	Bloomington Stock Center	62549	(Dunst et al., 2015)
Rab5-EYFP	Bloomington Stock Center	62543	Dunst et al., 2015
Rab7-EYFP	Bloomington Stock Center	62545	Dunst et al., 2015
UAS-Spastin (on II)	N. Sherwood, Duke		Sherwood et al., 2004
UAS-Spastin-CFP (on III)	N. Sherwood, Duke		Du et al., 2010
fkh-Gal4 (on II)	D. Andrew (John Hopkins University)		Chung et al., 2017
fkh-Gal4 (on III)	D. Andrew (John Hopkins University)		Chung et al., 2017
ubi-Rok-GFP	S. Parkhurst (Fred Hutchinson Cancer Research Center)		Abreu-Blanco et al., 2014
sqh-GFP			Royou et al., 2004

UAS-Rab11S25N-EYFP	Bloomington Stock Center	9792, 23261	
UAS-Dicer-2	Bloomington Stock Center	60008	
UAS-Dhc64C RNAi	Bloomington Stock Center Vienna *Drosophila* Resource Center	76941, 28749, v28053, v28054. 4 lines worked equally. v28054 was used for all of the data shown in this work.	
klar[1]	Bloomington Stock Center	3256	
klar[mCD4]	Bloomington Stock Center	25097	
klar[mCD4] ubi-Rok-GFP	Recombinant line generated from *klar[mCD4]* and *ubi-Rok-GFP*		
UAS-Crb RNAi	Bloomington Stock Center	38373, 38903, 40869, 34999.	

		4 lines worked equally. 2 lines (38373, 34999) were used for the data shown in this work.	
UAS-Baz RNAi	Bloomington Stock Center	35002, 38213, 39072. 38213 provided the strongest phenotype and used for quantification in this work.	
UAS-E-Cad RNAi	Bloomington Stock Center	32904	
UAS-Shg-GFP	Bloomington Stock Center	58445	
UAS-Baz-GFP	Bloomington Stock Center	65845	
matα-Gal4 (*maternal Gal4*; on II)	Bloomington Stock Center	7062	

560

561

Antibody	Source	RRID	Dilution
α-E-Cad (rat)	DSHB (deposited by T. Uemura, Kyoto University)	DCAD2 (AB_528120)	1:50
α-CrebA (rat)	Andrew lab (John Hopkins University)		1:3000
α-CrebA (rabbit)	Andrew lab (John Hopkins University)		1:5000
α-Dhc (mouse)	DSHB (deposited by J.M. Scholey, University of California)	2C11-2 (AB_2091523)	1:50
α-Rab11 (rabbit)	Andrew lab (John Hopkins University)		1:500
α-Nuf (guinea pig)	Sotillos lab (CABD)		1:500
α-acetylated α-tubulin (mouse)	Invitrogen	32-2700 (AB_2533073)	1:1000
α-tyrosinated α-tubulin (rat)	Invitrogen	MA1-80017 (AB_2210201)	1:1000
α-GFP (chick)	Invitrogen	A10262 (AB_2534023)	1:500

α-β-galactosidase (rabbit)	Invitrogen	A11132 (AB_221539)	1:500
α-Crb (mouse)	DSHB (deposited by E. Knust, Max Planck Institute)	Cq4 (AB_528181)	1:10
α-Fog (rabbit)	N. Fuse (Fuse et al., 2013)		1:1000
α-Sec15 (guinea pig)	Bellen lab (Baylor College of Medicine)		1:2000
Alexa Fluor 488/568/647-coupled secondary antibodies	Invitrogen		1:500

562

563 **Acknowledgments**

571

572   **Figure legends**

573   **Figure 1. Intracellular trafficking components are apically enriched near the**

574   **invagination pit.** (A) A schematic drawing of the anterior region of the *Drosophila* embryo

575   for stage 11 (ventral and lateral views) and stage 16 (lateral view). Green, SGs. Top right,

576   magnified view of a SG placode. Purple area, the region where SG cells undergo

577   clustered apical constriction during invagination. (B-D) En face (top) and lateral (bottom)

578   views of a wild type SG immunostained for E-Cad, Rab11 and Nuf. Rab11 and Nuf show

579   apical upregulation near the invagination pit (yellow arrowheads). Red arrowheads,

580   Rab11 and Nuf signals near the segmental groove. (B'-D') Heat maps of apical area (B')

581   and intensity of Rab11 and Nuf (C', D'). Cells with small apical areas (dark blue cells in

582   B') near the invagination pit show high intensity of Rab11 and Nuf (red cells in C' and D').

583   (E) Negative correlation between Rab11/Nuf intensities and apical areas of SG cells. R,

584   Pearson correlation coefficient. p<0.0001 for all samples (n=5 SGs; 690 cells). (F-H')

585   *Rab11-EYFP* (an EYFP insertion at the N-terminus under the control of Rab11 regulatory

586   sequences) SG labeled with antibodies against E-Cad (F), GFP (G) and Nuf (H) and

587   corresponding heat maps for apical areas (F') and intensity of GFP (G') and Nuf signals

588   (H'). Rab11-EYFP shows the same enrichment near the invagination pit (F'-H'). (I-J') En

589   face (top) and lateral (bottom) views of a wild type SG immunostained with E-Cad (I) and

590   Dhc64C (J) and corresponding heat maps for apical areas (I') and intensity of Dhc64C

591   signals (J'). Yellow arrowheads, apical upregulation of Dhc64C near the invagination pit.

592   (K-L') A *Rab7-EYFP* (an EYFP insertion at the N-terminus under the control of Rab7

593   regulatory sequences) SG immunostained with E-Cad (K) and GFP (L) and

594   corresponding heat maps for apical areas (K') and intensity of Rab7-EYFP (L'). Asterisks:

595   invagination pit. White lines: SG boundary.

596

Figure 1

597
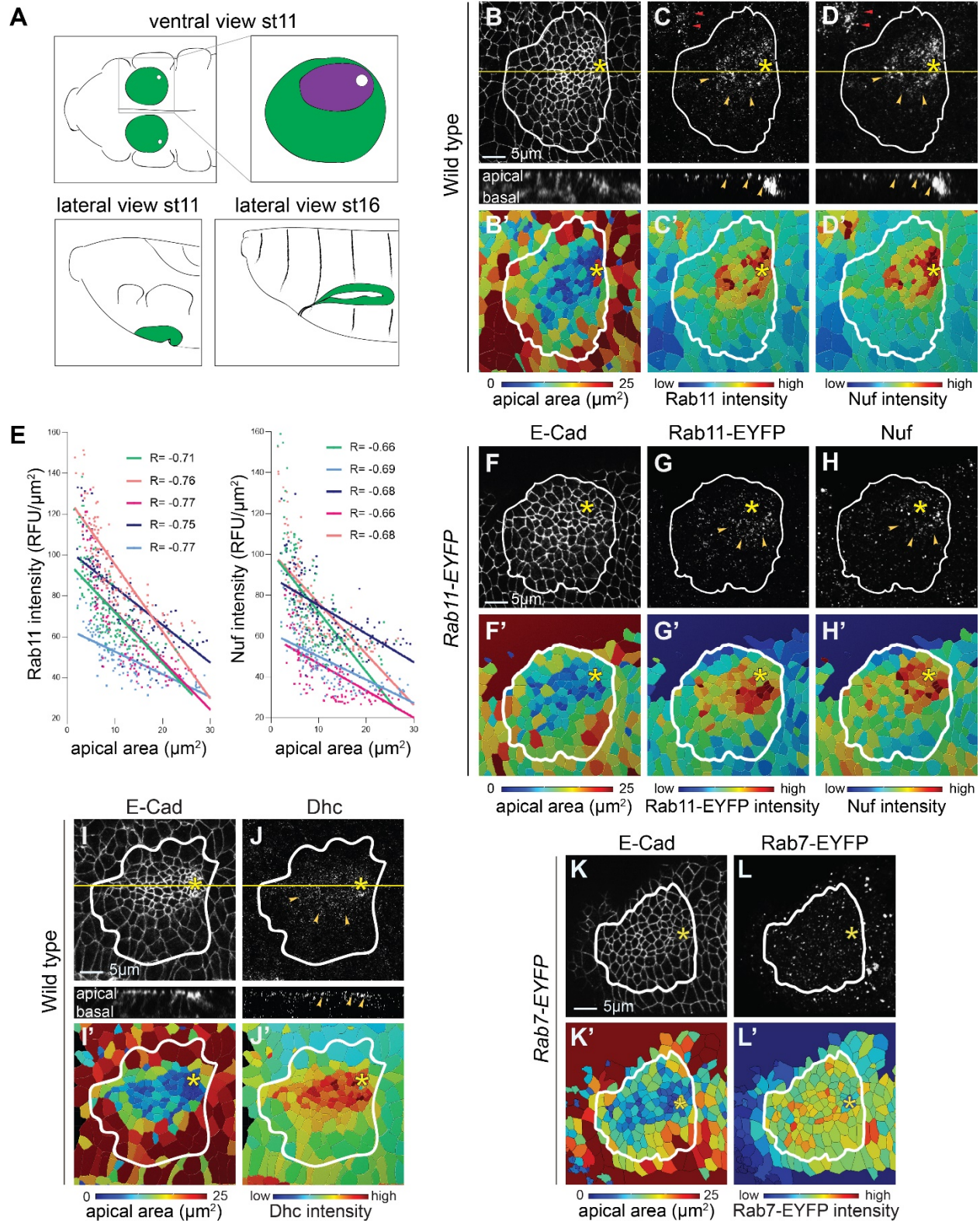
598   **Figure 2. Disruption of MTs results in uncoordinated apical constriction, reduction**

599   **of apical vesicle numbers, and mislocalization of Rab11/Nuf.** (A-A''') Co-localization

600   of Rab11 and tyrosinated α-tubulin in SG cells during invagination. A wild type SG

601   immunostained with Rab11 (green) and tyrosinated α-tubulin (purple; Tyr-α-Tub) is shown

602   with higher magnification of the yellow boxed area (A'-A'''). Yellow arrowheads, co-

603   localized Rab11 and tyrosinated α-tubulin. (B-B'') Z sections along the yellow line in (A).

604   Yellow arrowheads, co-localized Rab11 and tyrosinated α-tubulin. (C) Thresholded

605   Manders' colocalization coefficients show the extent to which two proteins colocalize (n=

606   6 SGs). (D-E''') Overexpression of spastin in the SG disrupts the MT networks and

607   compromises enrichment of Rab11 near the invagination pit. (D-D''') En face (top) and

608   lateral (bottom) views of a control SG show abundant levels of tyrosinated α-tubulin (D'')

609   and acetylated α-tubulin (D'''; Ace-α-Tub). Rab11 is enriched in the apical domain near

610   the invagination pit (yellow arrowheads). (E-E''') Overexpression of spastin by *fkh-Gal4*

611   leads to a loss of MTs in the SG, labelled both by tyrosinated α-tubulin (E'') and acetylated

612   α-tubulin (E'''). (E') Rab11 is not enriched near the invagination pit and mislocalizes

613   basolaterally when spastin is overexpressed (red arrowheads). (F-F'') Confocal images

614   of a spastin-overexpressing SG stained with Rab11 (F') and Nuf (F'') and corresponding

615   heat maps for apical areas (G), intensities of Rab11 (G') and Nuf (G''). Compare to control

616   SGs in Figure 1B-1H'. (H) A ratio of deviation of intensity to the median intensity of Rab11

617   (left) and Nuf (right) in all SG cells (n= 5 SGs; 690 cells). *, $p < 0.01$. ****, $p < 0.0001$, Mann-

618   Whitney U test. Asterisks: invagination pit. White lines: SG boundary.

Figure 2

619
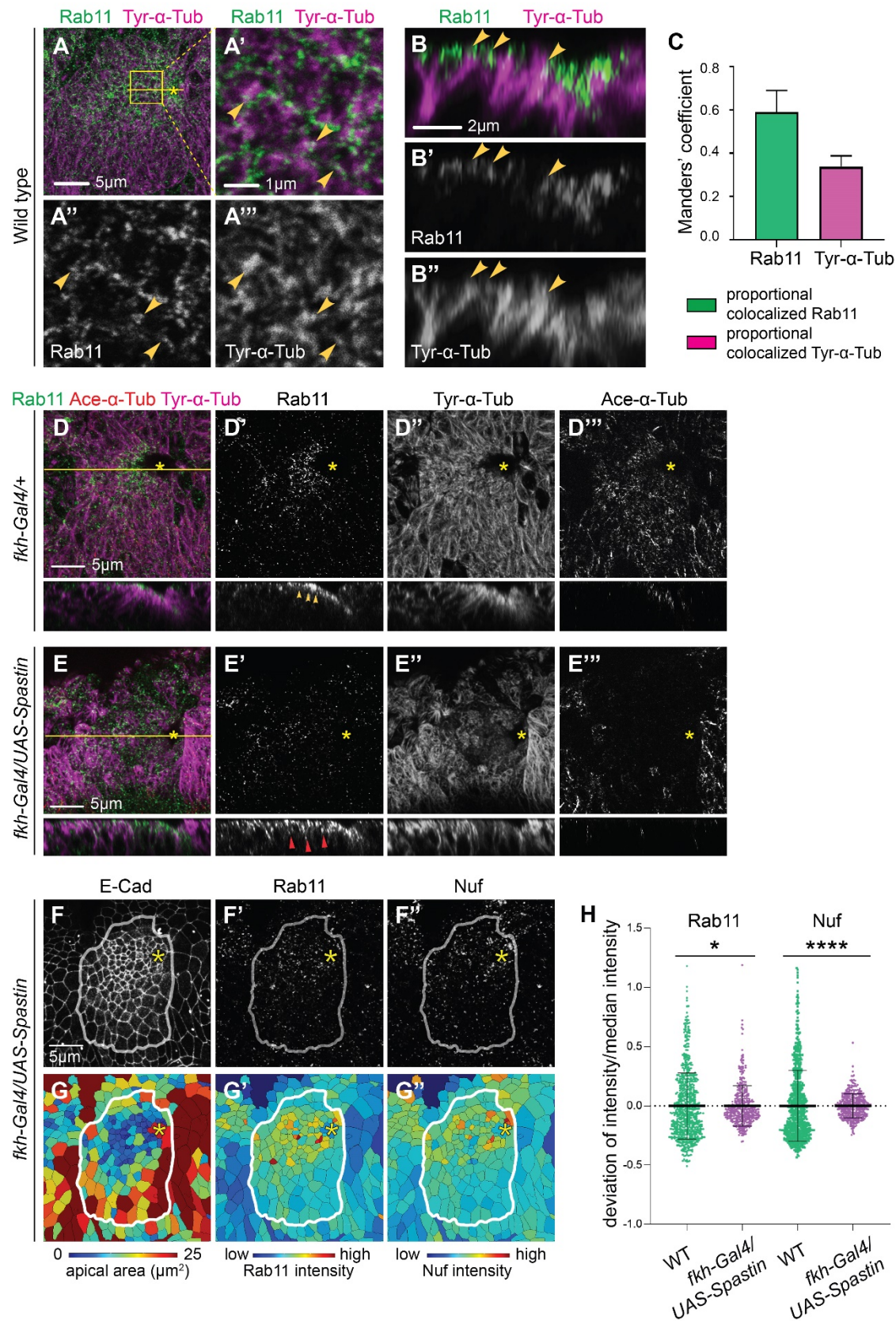
620 **Figure 3. Rab11 and the dynein motor are required for coordinated apical**

621 **constriction in the SG.** (A-C) Confocal images of control (A), Rab11-DN-overexpressing

622 (B) and *Dhc64C* RNAi (C) SGs immunostained with E-Cad. (A'-C') Heat maps

623 corresponding to images shown in A-C. (D-E') Confocal images and corresponding heat

624 maps of wild type (D, D') and *klar* mutant (E, E') SGs. (F, H) Percentage and cumulative

625 percentage of cells with different apical areas. Mann-Whitney U test (for percentage of

626 cells) and Kolmogorov-Smirnov test (for cumulative percentage of cells). n= 5 SGs

627 (control (*fkh-Gal4/+*), 517 cells; *Rab11-DN*, 536 cells; zygotic *Dhc64C* RNAi, 499 cells;

628 WT, 690 cells; *klar^1*, 705 cells; maternal/zygotic *Dhc64C* RNAi, 561 cells). **, $p<0.01$; ****,

629 $p<0.0001$. (G) A range of phenotypes is observed when *Dhc64C* is knocked down both

630 maternally and zygotically, including mild (uncoordinated apical constriction),

631 intermediate (enlarged pit) and severe (deformed epithelial tissue and additional folds)

632 phenotypes. Asterisks: invagination pit. White lines: SG boundary. (H) Percentage and

633 cumulative percentage of cells with different areas in SGs that were knocked down

634 *Dhc64C* both maternally and zygotically.

32

635

Figure 3

636

637

638
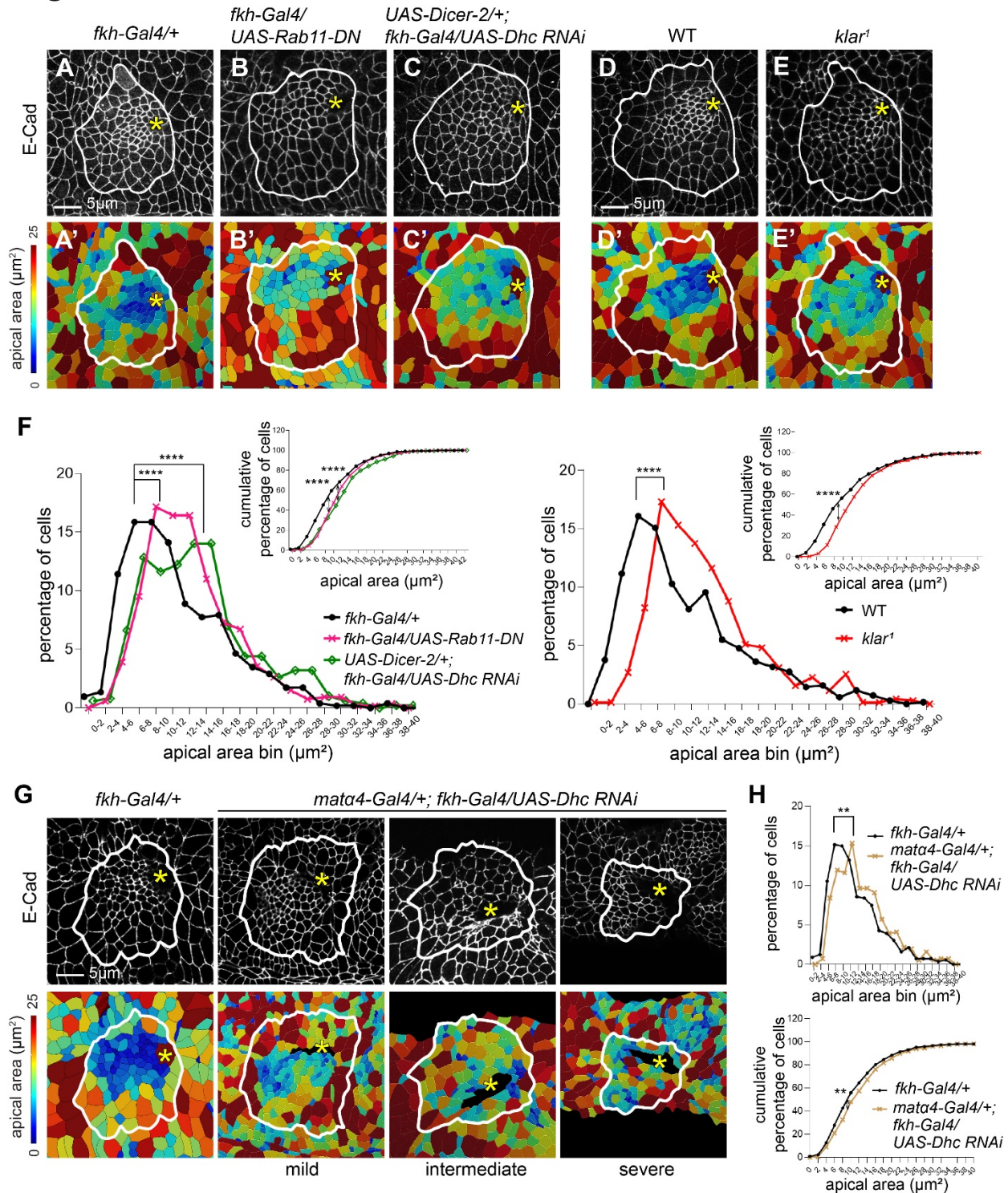
639 **Figure 4. Compromised dynein functions lead to a reduction of apicomedial myosin**

640 **formation in the SG cells.** (A-B'''') sqh-GFP signals in control (A-A'''') and *Dhc64C* RNAi

641 (B-B'''') SGs. (A''-B'''') Higher magnification of the yellow boxed area in A and B. *Dhc64C*

642 knockdown leads to reduced apicomedial myosin (red arrowheads in B'') compared to

643 strong signals of apicomedial myosin in A'' (yellow arrowheads). (C) Quantification of

644 apicomedial myosin, junctional myosin and the ratio of apicomedial to junctional myosin

645 in *Dhc64C* RNAi SG cells. (D-E'''') Myosin signals in control (D-D'''') and in *klar* mutant

646 (E-E'''') SGs. (D''-E'''') Higher magnification of the yellow boxed area in D and E. *Dhc64C*

647 knockdown leads to reduced apicomedial myosin (red arrowheads in E''); compare these

648 to strong signals of apicomedial myosin in D'' (yellow arrowheads). (F) Quantification of

649 apicomedial myosin, junctional myosin and the ratio of apicomedial to junctional myosin

650 in control and *klar* mutant SG cells. n= 5 SGs for all genotypes; 10 cells in the

651 dorsal/posterior region of each SG. *, $p < 0.05$. **, $p < 0.01$. ***, $p < 0.001$. ****, $p < 0.0001$,

652 Mann-Whitney U test. Asterisks: invagination pit.

34

Figure 4

653

35
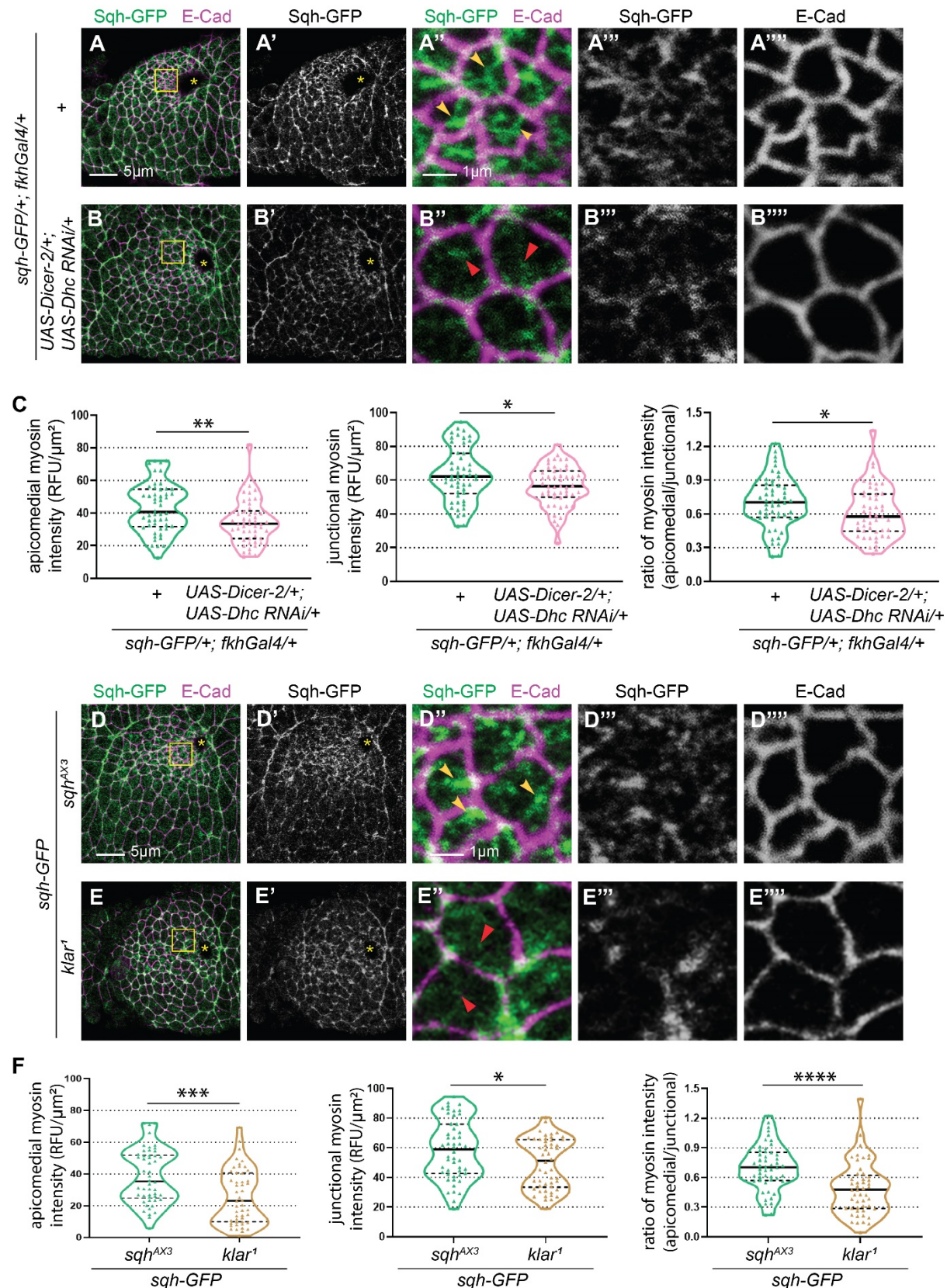
654 **Figure 5. Compromised MTs and dynein functions impair accumulation of**
655 **apicomedial Rok within constricting cells during invagination.** (A-A'') A control SG
656 shows accumulation of Rok-GFP signals (green) in the apicomedial region of cells near
657 the invagination pit. E-Cad (magenta), cell boundary. Yellow arrowheads, accumulative
658 Rok-GFP. (B-C'') Rok-GFP signals are more dispersed in SG cells upon spastin
659 overexpression (B-B'') and knockdown of *Dhc64C* (C-C'') (red arrowheads). (D) A control
660 SG homozygous for ubi-Rok-GFP shows a huge accumulation of Rok-GFP in constricting
661 cells (yellow arrowheads). (E) A mutation in *klar* results in slightly reduced accumulation
662 of Rok-GFP in cells near the invagination pit (red arrowheads). (F) Representative images
663 for how areas of Rok-GFP puncta were measured using the Fiji software. (G,H)
664 Quantification of areas of Rok-GFP puncta. ****, p< 0.0001, Mann-Whitney U test. n= 5
665 SGs for all genotypes; 15 cells in the dorsal/posterior region for each SG.
666
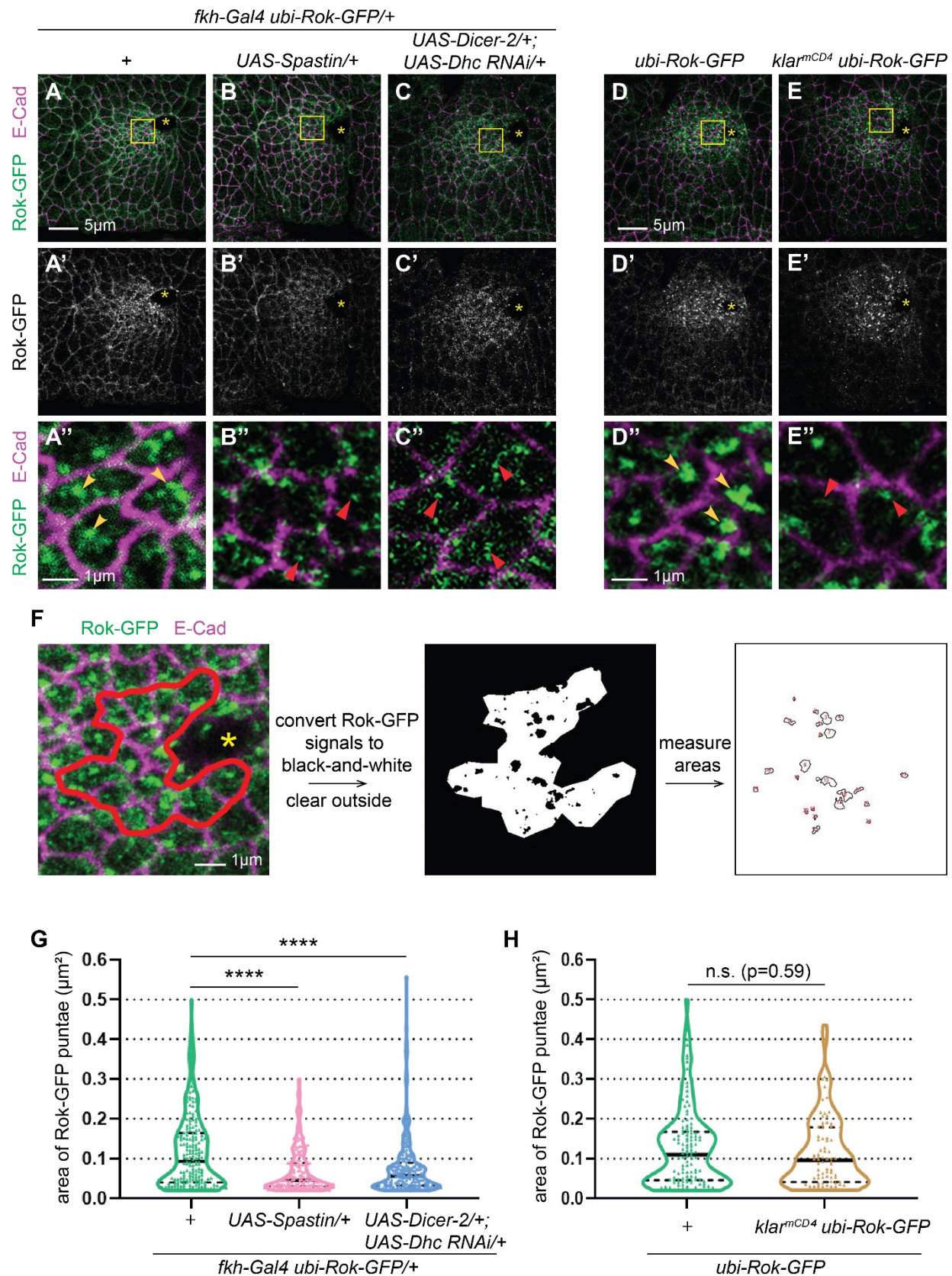
Figure 5

668 **Figure 6. Impairing MTs and dynein motors suppresses the over-active Fog**
669 **signaling pathway.** (A-A') Rok-GFP signals in constricting cells in a control SG (yellow
670 arrowheads). (B-B') In Fog-overexpressing SGs, Rok-GFP is over-accumulated in cells
671 (red arrowheads). (C-D') The Rok over-accumulation phenotype is suppressed when
672 spastin is overexpressed or *Dhc64C* is knocked down (red arrows). (E-E') Apicomedial
673 myosin in the control SG (yellow arrowheads). (F-F') Fog-overexpressing SG cells show
674 increased apicomedial myosin (red arrowheads). (G-H') Upregulation of apicomedial
675 myosin caused by Fog overexpression is inhibited when spastin is overexpressed or
676 *Dhc64C* is knocked down (red arrows). (I-I') Fog overexpressing SG cells show wavy
677 adherens junctions (E-Cad) signals. Cell junctions are deformed at the contact sites to
678 apicomedial myosin (red arrowheads). (J) Quantification of areas of Rok-GFP puncta. (n=
679 5 SGs; 15 cells for each SG). (K) Left, a cartoon for how the tortuosity of a cell junction
680 was measured. Right, quantification of the tortuosity (n= 5 SGs; 10 cells for each SG;
681 ~280 junctions). (L) Quantification of apicomedial myosin, junctional myosin and the ratio
682 of apicomedial to junctional myosin (n= 5 SGs; 10 cells for each SG). For all quantification,
683 cells in the dorsal/posterior region of SG placode were used. *, $p< 0.05$. **, $p< 0.01$. ***,
684 $p< 0.001$. ****, $p< 0.0001$, Mann-Whitney U test. Asterisks: invagination pit.

38
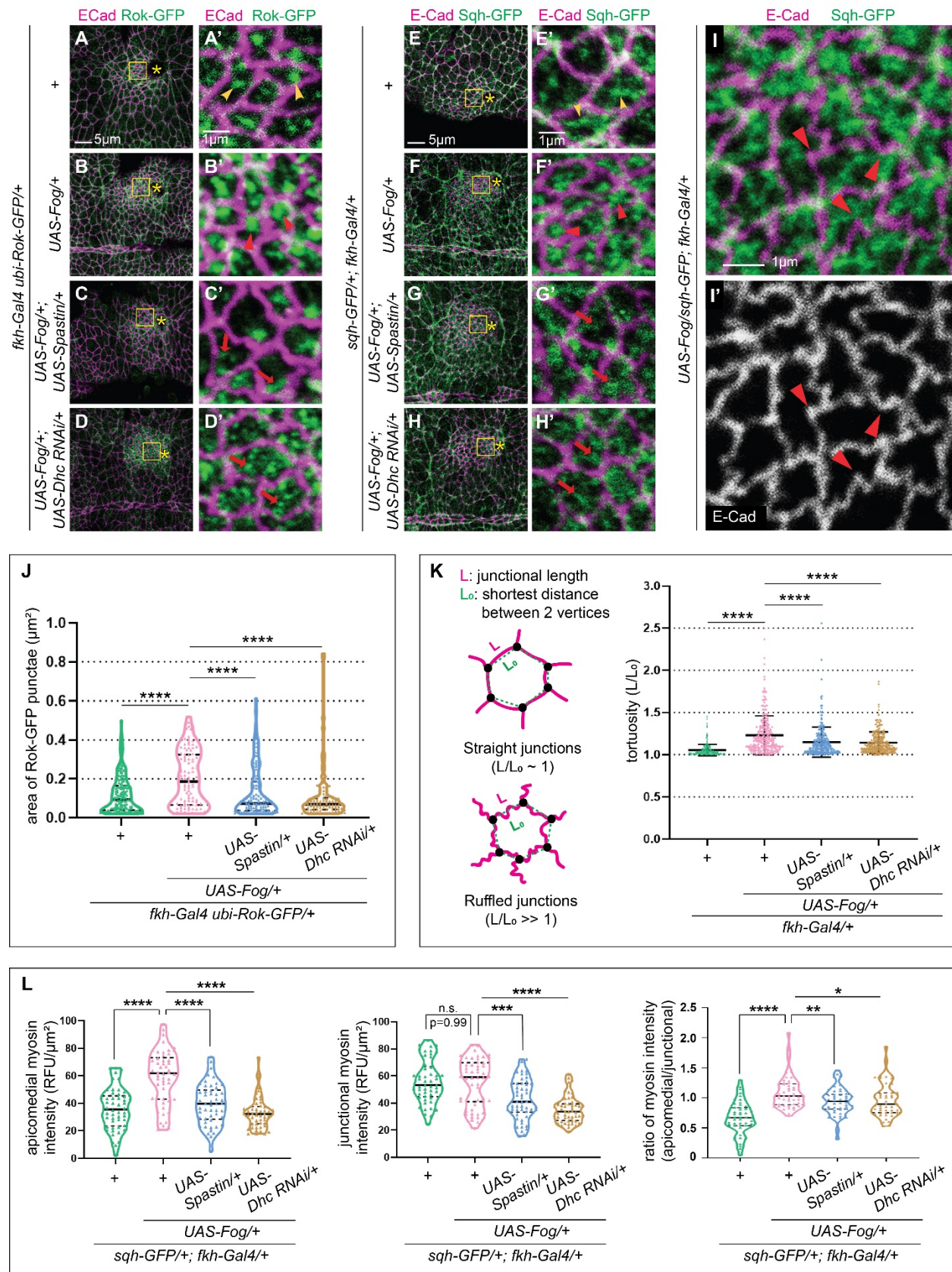
Figure 6

686 **Figure 7. Crb, E-Cad and Baz have a role in regulating apical constriction during**

687 **SG invagination.** (A-B'') Control and spastin-overexpressing SGs immunostained with

688 E-Cad and Crb. (C-D') Higher magnification of boxed areas in A' and B'. Crb staining

689 shows gaps along the junctions in spastin-overexpressing SGs (yellow arrows). (E,F)

690 Control and spastin-overexpressing SGs immunostained with Baz. (G-I) Quantification of

691 junctional signals for Crb (G), E-Cad (H) and Baz (I). n= 3 SGs; 30 cells for each SG. (J,

692 K) Quantification of the ratio of length of gaps to junctional length (J; Mann-Whitney U

693 test) and the number of gaps (K; Student t-test) in SGs immunostained with Crb. n= 4

694 SGs; 10 cells for each SG. (L-O') Confocal images of SGs stained with E-Cad (L-O) and

695 corresponding heat maps for apical areas (L'-O'). (H) Percentage and cumulative

696 percentage of cells with different apical areas. Mann-Whitney U test (percentage of cells)

697 and Kolmogorov-Smirnov test (cumulative percentage of cells). n= 5 SGs (control, 517

698 cells; *crb* RNAi, 583 cells; *E-Cad* RNAi, 712 cells; *baz* RNAi, 601 cells). *, p<0.05. **,

699 p<0.01, ****, p<0.0001. Asterisks: invagination pit.

40
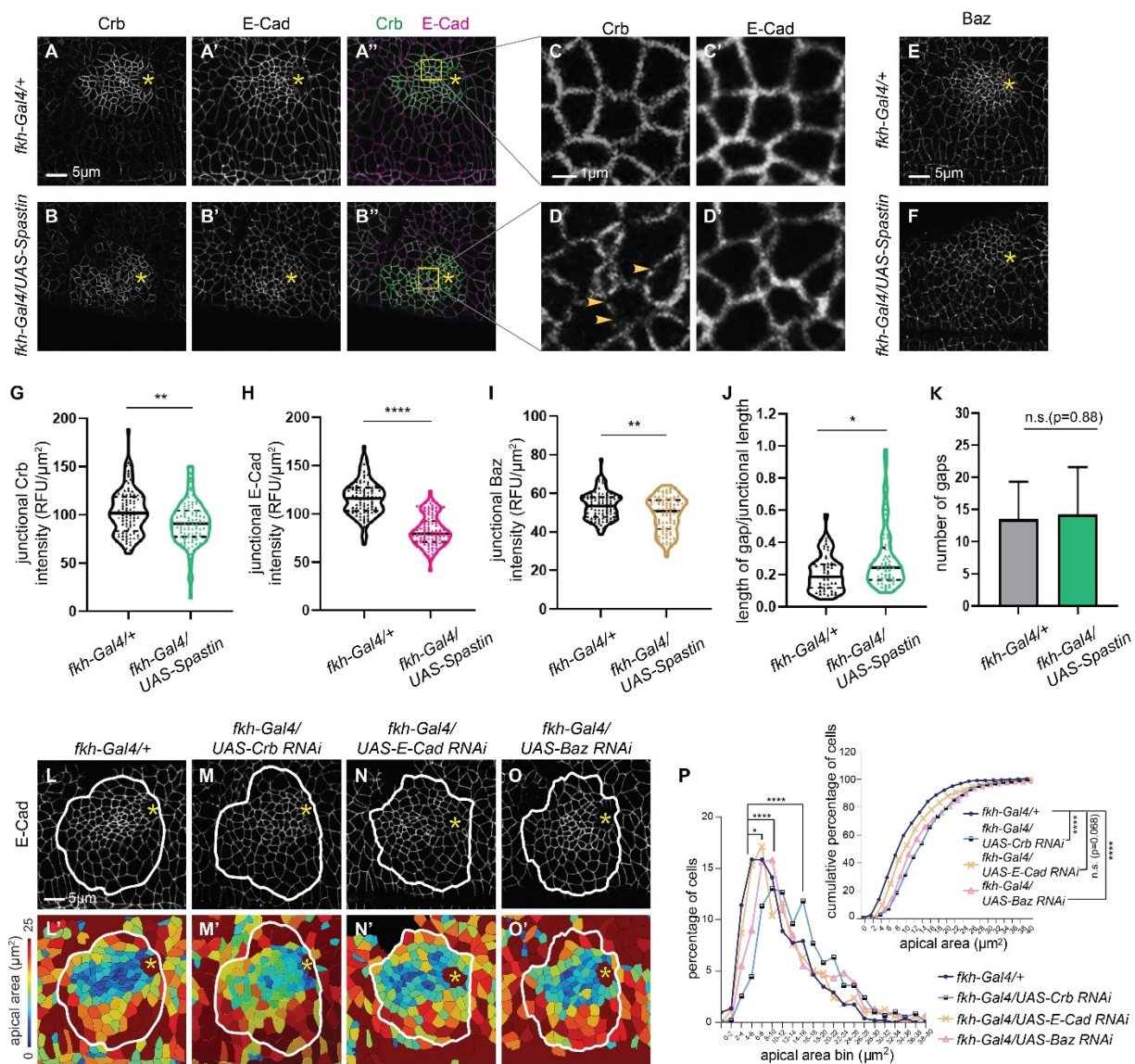
Figure 7

703 **Figure 8. Knockdown of *crb*, *E-Cad* or *baz* results in reduced apicomedial myosin**

704 **formation and dispersed apicomedial Rok.** (A-D") Compared to strong apicomedial

705 myosin in control SGs (yellow arrowheads in A''), knockdown of *crb*, *E-Cad* or *baz* results

706 in reduction of apicomedial myosin in SG cells near the invagination pit (red arrowheads

707 in B''-D''). (A"-D") Higher magnification of yellow boxed areas shown in A-D. (E)

708 Quantification of apicomedial myosin, junctional myosin and ratio of apicomedial to

709 junctional myosin of SG cells from different genotypes shown in A-D (n=5 SGs for each

710 genotype; 10 cells in the dorsal/ posterior region). **, $p<0.01$. ***, $p< 0.001$. ****, $p<0.0001$.

711 Mann-Whitney U test. (F-I'') Compared to Rok accumulation in control SGs (yellow

712 arrowheads in F''), reduction of *crb*, *E-Cad* or *baz* causes less accumulating Rok-GFP

713 signals in the apical domain of cells near the pit (red arrowheads in G''-I''). (F''-I'') Higher

714 magnification of yellow boxed areas shown in F-I. (J) Quantification of areas of Rok-GFP

715 puncta in SG cells from different genotypes shown in F-I (n=5 SGs; 15 cells in the

716 dorsal/posterior for each genotype). **, $p< 0.01$. ****, $p< 0.0001$. Mann-Whitney U test.
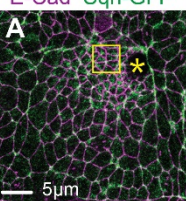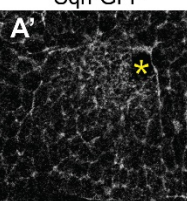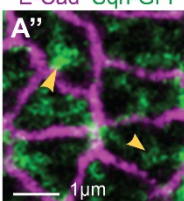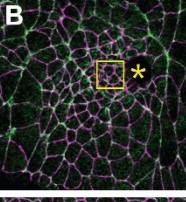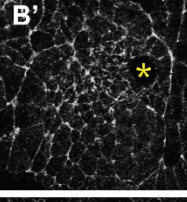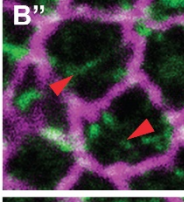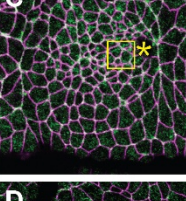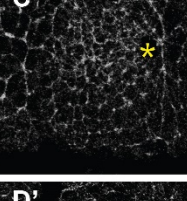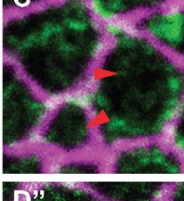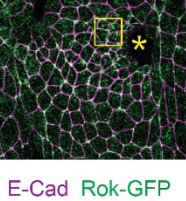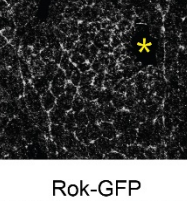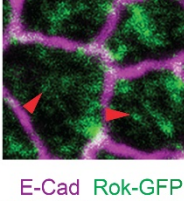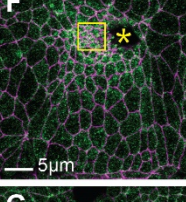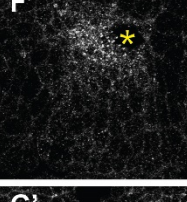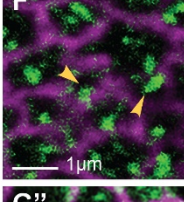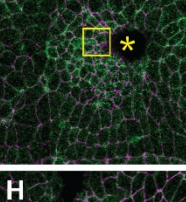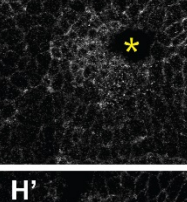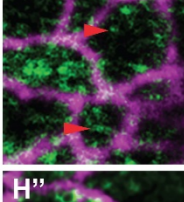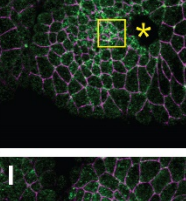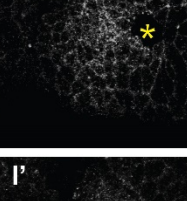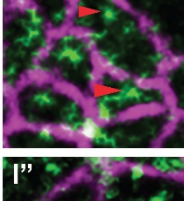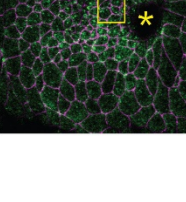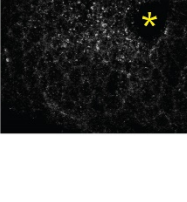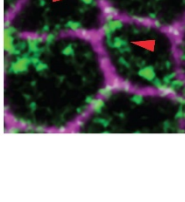
717 Asterisks: invagination pit.

42

Figure 8

718

719 **Figure 9. A proposed model for MT-dependent trafficking to promote apical**

720 **constriction during SG invagination.** Vesicular transport is essential for apical

721 localization of Crb, E-Cad, and Baz to regulate apical myosin networks and subsequent

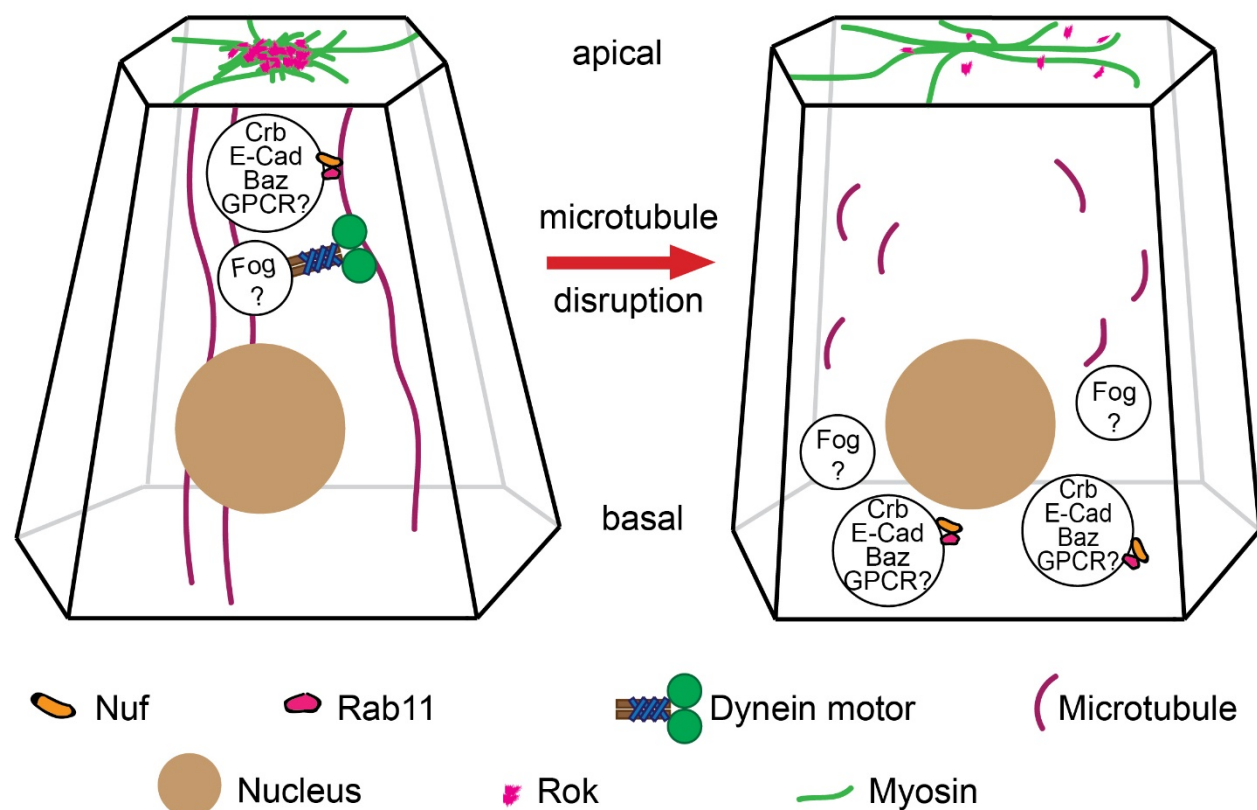722 apical constriction. Fog signaling activity also depends on MTs and dynein motors.

723

724

725

Figure 9

726

727

728   **Figure S1. Sec15 and Rab5-EYFP are enriched near the invagination pit during SG**

729   **invagination.** (A-B') Confocal images of a Rab5-EYFP SG stained with E-Cad (A) and

730   GFP (B). Rab5-EYFP is an EYFP insertion at the N-terminus under the control of Rab5

731   regulatory sequences. GFP signals are upregulated in the apical region near the

732   invagination pit. (A', B') Heat maps of apical areas (A') and intensity of Rab5-EYFP signals

733   (B'). Cells with small apical areas (dark blue cells in A') near the invagination pit show

734   high intensity of Rab5-EYFP (red cells in B'). (C) Negative correlation between Rab5-

735   EYFP intensity and apical areas of SG cells (n= 4 SGs; 396 cells). (D-E') Sec15 is

736   upregulated in the cells near the invagination pit. (D, E) Wild type embryo immunostained

737   with E-Cad and Sec15. (D', E') Heat maps of apical areas (D') and intensity of Sec15

738   signals (E'). (F) Negative correlation between intensity of Sec15 and apical areas of SG

739   cells (n= 5 SGs; 527 cells). Asterisks: invagination pit.

Supplemental Figure 1

740
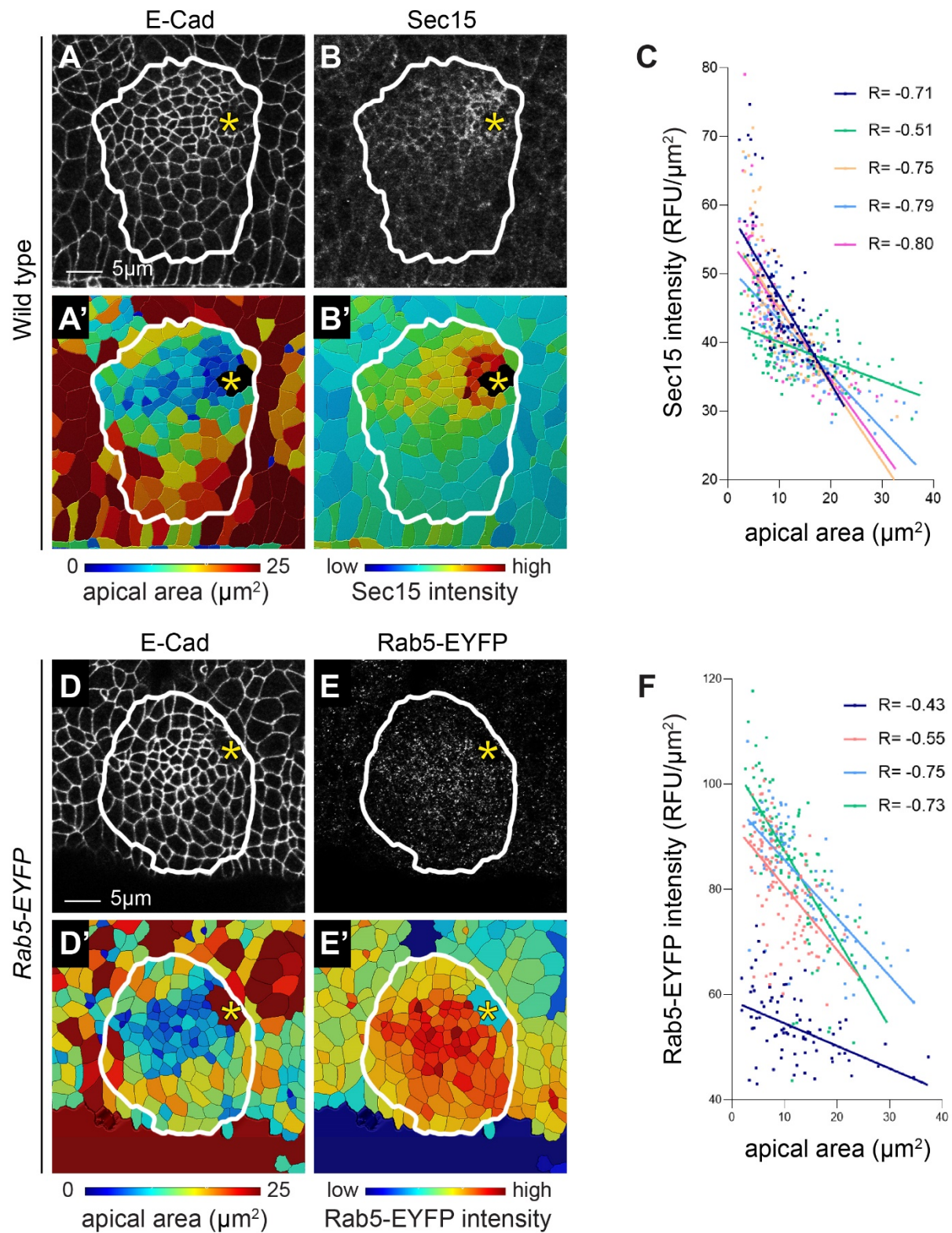
741 **Figure S2. Overexpression of spastin results in loss of acetylated-α-tubulin in SG**

742 **cells.** (A-B'') Confocal images of a control (A-A'') and spastin-CFP-overexpressing SG

743 (B-B'') stained with phalloidin (red) and acetylated α-tubulin (magenta). Spastin-CFP

744 (green) signals show SG-specific overexpression of spastin by fkh-Gal4, which leads to

745 a loss of MTs in that region. Asterisks, invagination pit.

746

747

Supplemental Figure 2

748
749

750

Supplemental Figure 3

fkh-Gal4/+ *UAS-Crb/+;* *UAS-Crb/+;*
fkh-Gal4/+ *fkh-Gal4/UAS-Spastin*

751
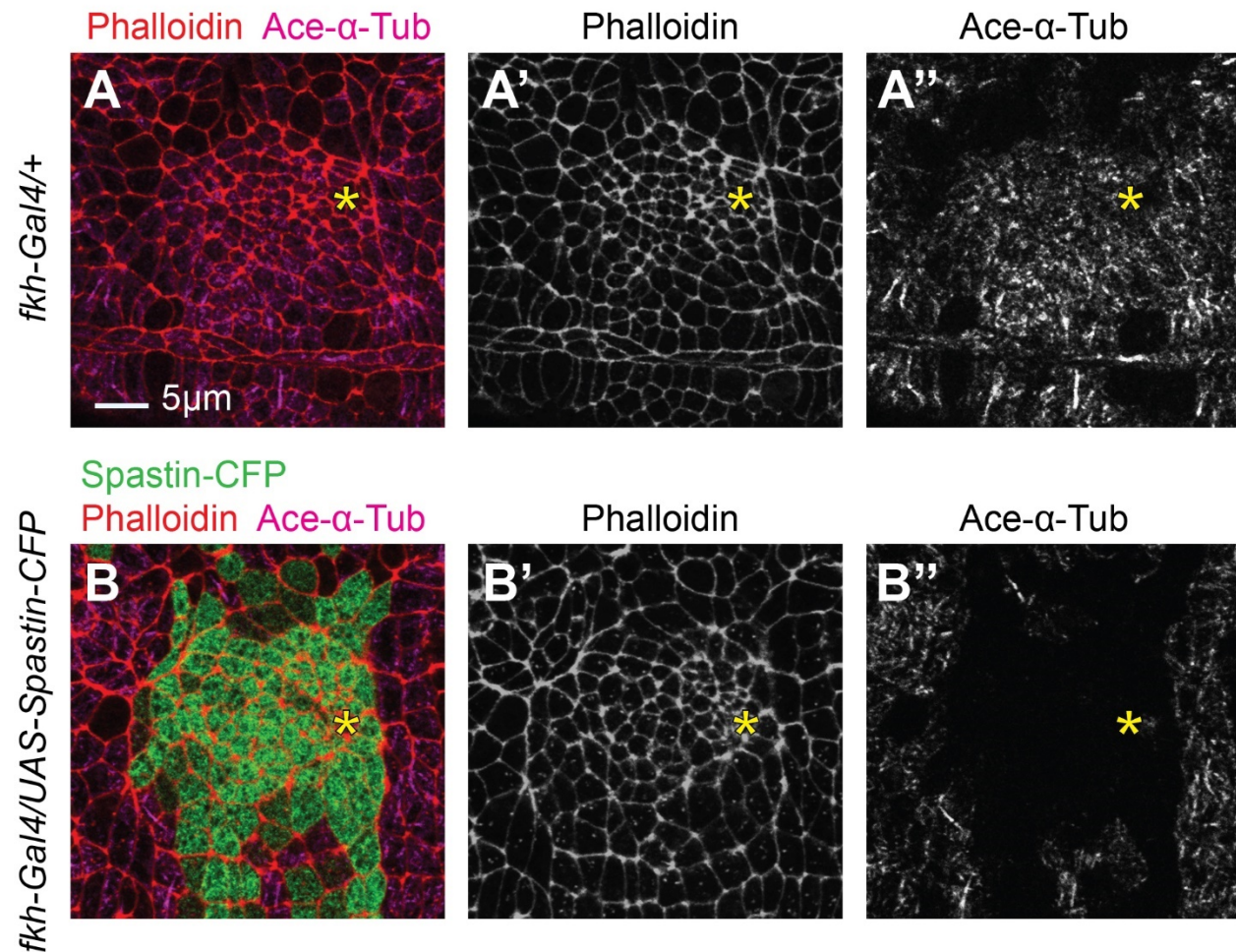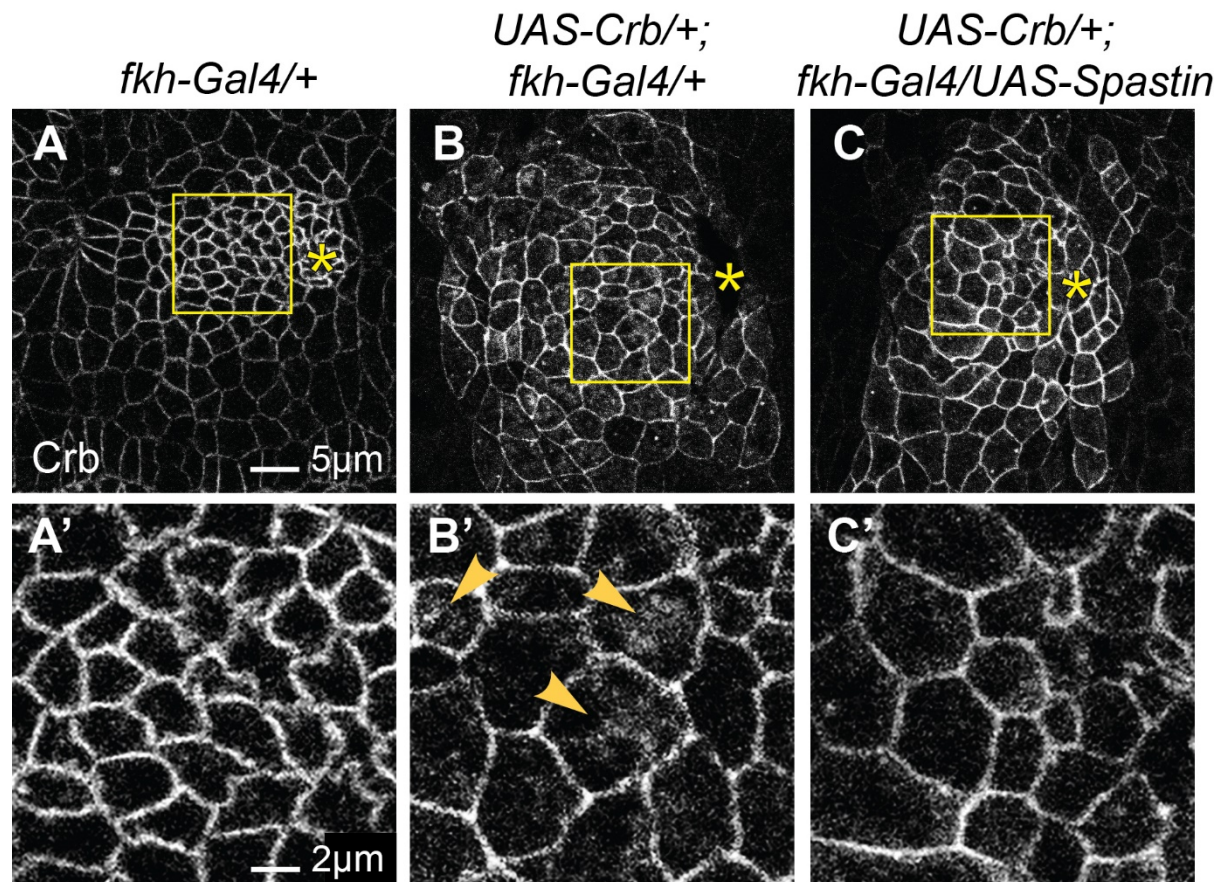
752   **Figure S4. Knockdown of *crb*, *E-Cad* and *baz* reduces Crb, E-Cad and Baz levels in**

753   **the SG.** (A-C'') Compared to strong Crb, E-Cad and Baz signals in control SGs (A-C),

754   knockdown of *crb*, *E-Cad* and *baz* results in reduction of Crb, E-Cad and Baz levels in

755   SG cells near the invagination pit (A'-C'). (A''-C'') Quantification of junctional intensity of

756   Crb, E-Cad and Baz. n=5 SGs (10 cells in the dorsal/posterior region of each SG were

757   tested). ****, p< 0.0001 (Mann-Whitney U test). Asterisks, invagination pit.

758

Supplemental Figure 4

759

760
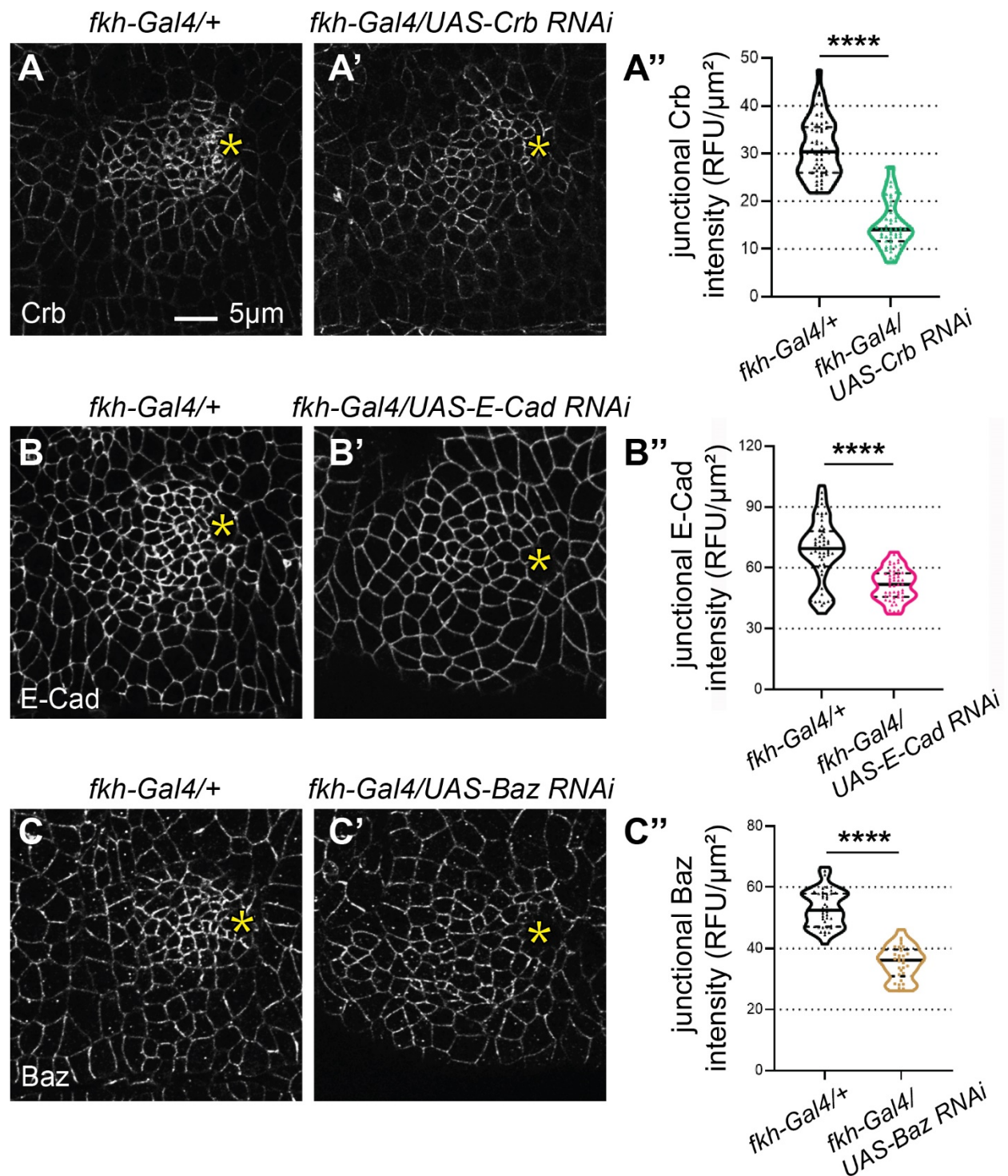
761 **Figure S5. MTs play a role in trafficking key apical and junctional proteins during**

762 **SG formation.** (A-B''') Overexpression of spastin results in mislocalization of Rab11 and

763 Nuf in stage 16 SGs. (A-A''') In control, Rab11 and Nuf localize in the apical region of SG

764 cells (red arrowheads). (B-B''') In spastin-overexpressing SGs, Rab11 and Nuf are

765 mislocalized to aggregates in the cytoplasm of cells (yellow arrowheads). (C-C''')

766 Overexpression of Crb causes mislocalization of Crb in all membrane domains and

767 expands the membrane. Rab11 is still enriched in the apical domain (red arrowheads).

768 (D-D''') Co-overexpression of spastin and Crb results in mislocalization of Crb to large

769 aggregates in the cytoplasm, which overlap with Rab11 (yellow arrowheads). (E-E''')

770 Overexpression of E-Cad causes a slight increase of the apical membrane, with the

771 majority of E-Cad signals in the apical domain (red arrowheads) and only some punctate

772 E-Cad signals in the basolateral region (blue arrows). (F-F''') Co-overexpression of E-

773 Cad and spastin causes mislocalization of E-Cad to cytoplasmic aggregates, which

774 overlap with Nuf (yellow arrowheads). (G-G''') Overexpression of Baz causes a slightly

775 enlarged lumen. Red arrowheads, apical localization of Baz and Nuf. (H-H''') The

776 enlarged lumen phenotype caused by Baz overexpression is suppressed when spastin is

777 co-overexpressed. Blue arrows, a pool of mislocalized Nuf overlaps with mislocalized

778 Baz. Yellow arrowheads, mislocalized Nuf that does not overlap with Baz. White dashed

779 line, cell and nuclear boundaries (H) and apical membrane (I). Nu, nucleus.

780

Supplemental Figure 5

781
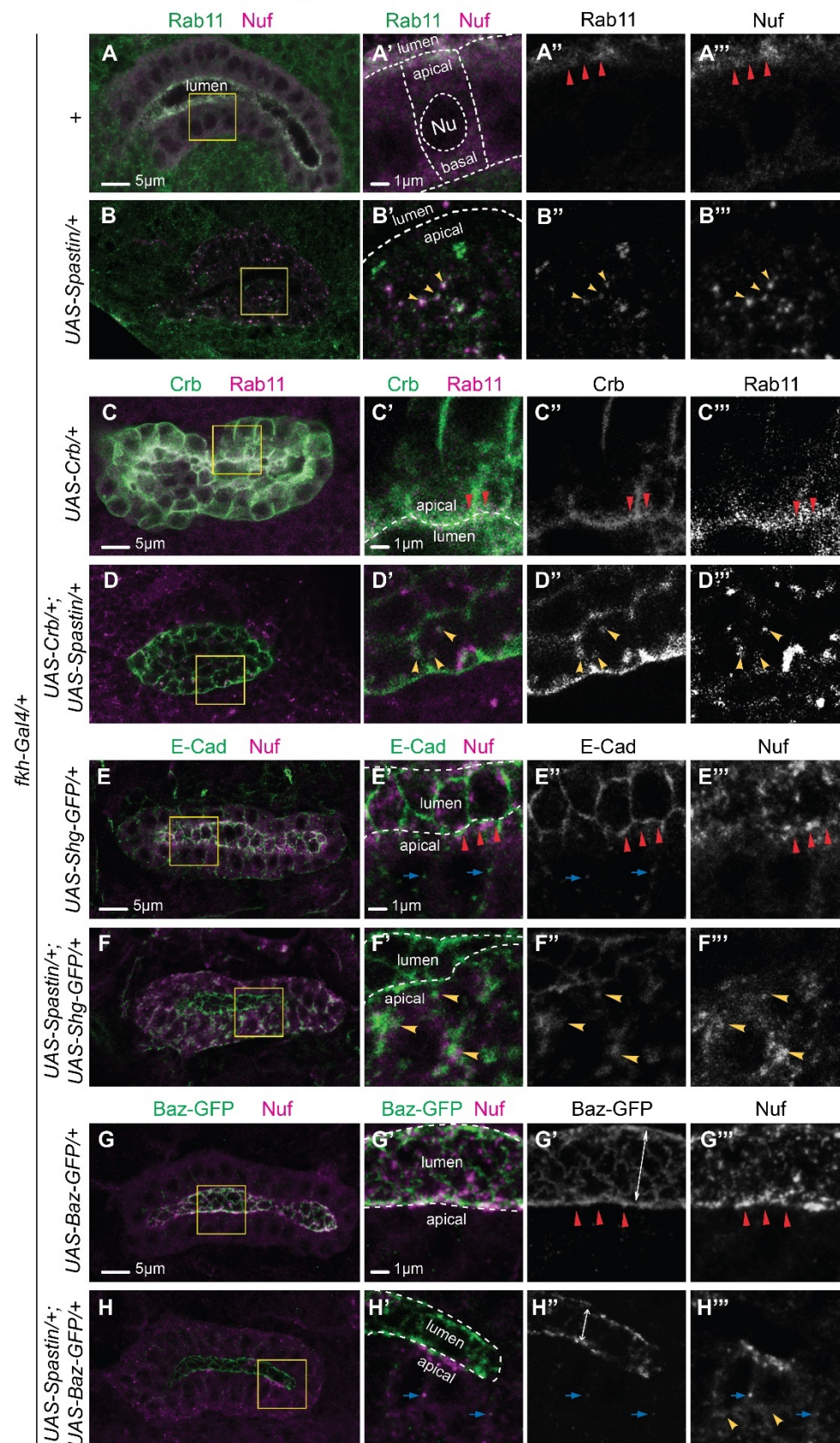
782 **Figure S6: Fog does not colocalize with Nuf when MTs are disrupted.** (A-A''') A stage
783 16 SG overexpressing Fog shows mislocalized Fog as cytoplasmic aggregates (yellow
784 arrowheads). Nuf is still apically localized (red arrowheads). (B-B''') When Fog and
785 spastin are co-overexpressed, mislocalized Fog is mainly observed in the basal region of
786 cells. Nuf is mislocalized to the basolateral region of cells but does not overlap with Fog
787 (yellow arrowheads). Nu: nucleus.

788

789

Supplemental Figure 6

790
791
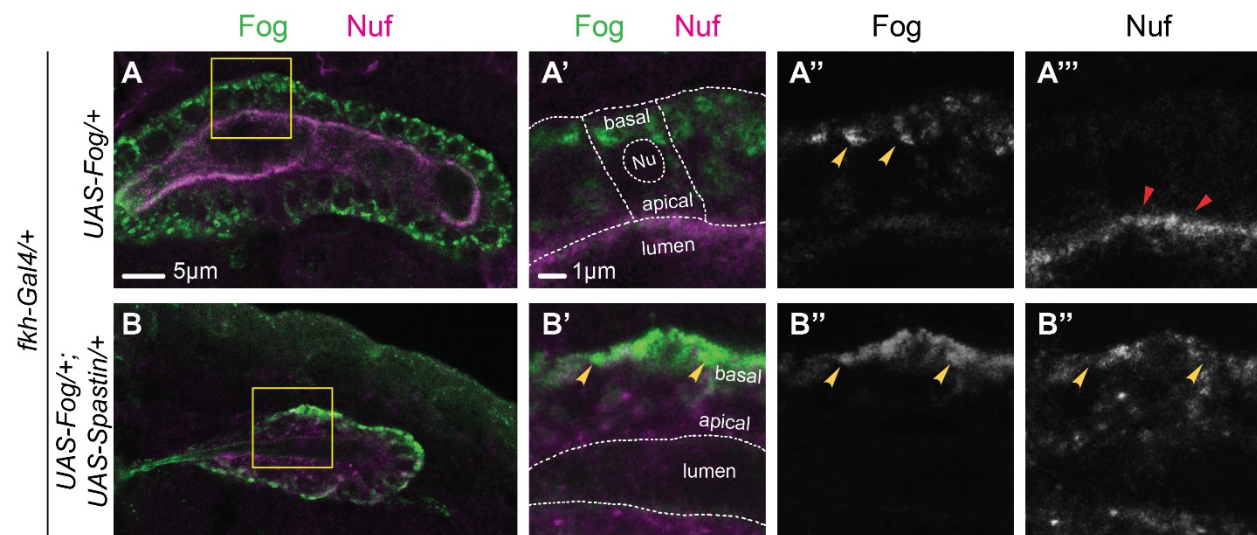
792 **Fly genotypes**

Figures	Genotypes
Figure 1B-D', I-J'	Oregon R
Figure 1F-H'	*Rab11-EYFP*
Figure 1K-L'	*Rab7-EYFP*
Figure 2A-B''	Oregon R
Figure 2D-D'''	*fkh-Gal4/+*
Figure 2E-E''', F-G''	*fkh-Gal4/UAS-Spastin-CFP*
Figure 3A-A'	*fkh-Gal4/+*
Figure 3B-B'	*fkh-Gal4/UAS-Rab11-S25N-YFP*
Figure 3C-C'	*UAS-Dicer-2/+; fkh-Gal4/UAS-Dhc64C RNAi*
Figure 3D-D'	Oregon R
Figure 3E-E'	*klar^1*
Figure 3G, first left panel (top and bottom)	*fkh-Gal4/+*
Figure 3G, three right panels (top and bottom)	*matα-Gal4/+; fkh-Gal4/UAS-Dhc64C RNAi*
Figure 4A-A''''	*sqh-GFP/+; fkh-Gal4/+*
Figure 4B-B''''	*sqh-GFP/UAS-Dicer-2; fkh-Gal4/UAS-Dhc64C RNAi*
Figure 4D-D''''	*sqh-GFP; sqh^{AX3}*
Figure 4E-E''''	*sqh-GFP; klar^1*

Figure 5A-A''	*fkh-Gal4 ubi-Rok-GFP/+*
Figure 5B-B''	*UAS-Spastin; fkh-Gal4 ubi-Rok-GFP/+*
Figure 5C-C''	*UAS-Dicer-2/+; fkh-Gal4 ubi-Rok-GFP/UAS-Dhc64C RNAi*
Figure 5D-D''	*ubi-Rok-GFP*
Figure 5E-E''	*klar^{mCD4} ubi-Rok-GFP*
Figure 5F	*fkh-Gal4 ubi-Rok-GFP/+*
Figure 6A-A'	*fkh-Gal4 ubi-Rok-GFP/+*
Figure 6B-B'	*UAS-Fog/+; fkh-Gal4 ubi-Rok-GFP/+*
Figure 6C-C'	*UAS-Fog/+; fkh-Gal4 ubi-Rok-GFP/UAS-Spastin*
Figure 6D-D'	*UAS-Fog/+; fkh-Gal4 ubi-Rok-GFP/UAS-Dhc64C RNAi*
Figure 6E-E'	*sqh-GFP/+; fkh-Gal4/+*
Figure 6F-F'	*sqh-GFP/UAS-Fog; fkh-Gal4/+*
Figure 6G-G'	*sqh-GFP/UAS-Fog; fkh-Gal4/UAS-Spastin*
Figure 6H-H'	*sqh-GFP/UAS-Fog; fkh-Gal4/UAS-Dhc64C RNAi*
Figure 6I-I'	*sqh-GFP/UAS-Fog; fkh-Gal4/+*
Figure 7A-A'', C-C', E	*fkh-Gal4/+*
Figure 7B-B'', D-D', F	*fkh-Gal4/UAS-Spastin*

55

Figure 7L-L'	*fkh-Gal4/+*
Figure 7M-M'	*fkh-Gal4/UAS-Crb RNAi*
Figure 7N-N'	*fkh-Gal4/UAS-E-Cad RNAi*
Figure 7O-O'	*fkh-Gal4/UAS-Baz RNAi*
Figure 8A-A''	*sqh-GFP/+; fkh-Gal4/+*
Figure 8B-B''	*sqh-GFP/+; fkh-Gal4/UAS-Crb RNAi*
Figure 8C-C''	*sqh-GFP/+; fkh-Gal4/UAS-E-Cad RNAi*
Figure 8D-D''	*sqh-GFP/+; fkh-Gal4/UAS-Baz RNAi*
Figure 8F-F''	*fkh-Gal4 ubi-Rok-GFP/+*
Figure 8G-G''	*fkh-Gal4 ubi-Rok-GFP/UAS-Crb RNAi*
Figure 8H-H''	*fkh-Gal4 ubi-Rok-GFP/UAS-E-Cad RNAi*
Figure 8I-I''	*fkh-Gal4 ubi-Rok-GFP/UAS-Baz RNAi*
Figure S1A-B'	*Oregon R*
Figure S1D-E'	*Rab5-EYFP*
Figure S2A-A''	*fkh-Gal4/+*
Figure S2B-B''	*fkh-Gal4/UAS-Spastin-CFP*
Figure S3A-A'	*fkh-Gal4/+*
Figure S3B-B'	*UAS-Crb/+; fkh-Gal4/+*
Figure S3C-C'	*UAS-Crb/+; fkh-Gal4/UAS-Spastin*

Figure S4A,B,C	*fkh-Gal4/+*
Figure S4A'	*fkh-Gal4/UAS-Crb* RNAi
Figure S4B'	*fkh-Gal4/UAS-E-Cad* RNAi
Figure S4C'	*fkh-Gal4/UAS-Baz* RNAi
Figure S5A-A'''	*fkh-Gal4/+*
Figure S5B-B'''	*fkh-Gal4/UAS-Spastin*
Figure S5C-C'''	*UAS-Crb/+; fkh-Gal4/+*
Figure S5D-D'''	*UAS-Crb/+; fkh-Gal4/UAS-Spastin*
Figure S5E-E'''	*fkh-Gal4/UAS-Shg-GFP*
Figure S5F-F'''	*UAS-Spastin/+; fkh-Gal4/UAS-Shg-GFP*
Figure S5G-G'''	*fkh-Gal4/UAS-Baz-GFP*
Figure S5H-H'''	*UAS-Spastin/+; fkh-Gal4/UAS-Baz-GFP*
Figure S6A-A'''	*UAS-Fog/+; fkh-Gal4/+*
Figure S6B-B'''	*UAS-Fog/+; fkh-Gal4/UAS-Spastin*

793

794

795

796

References

Aguilar-Aragon, M., G. Fletcher and B. J. Thompson (2019). Apical transport of Crumbs maintains epithelial cell polarity. Biorxiv.

Abreu-Blanco, M.T., Verboon, J.M., and Parkhurst, S.M. (2014). Coordination of Rho family GTPase activities to orchestrate cytoskeleton responses during cell wound repair. Curr Biol *24*, 144-155.

Anborgh, P.H., Seachrist, J.L., Dale, L.B., and Ferguson, S.S. (2000). Receptor/beta-arrestin complex formation and the differential trafficking and resensitization of beta2-adrenergic and angiotensin II type 1A receptors. Mol Endocrinol *14*, 2040-2053.

Andrew, D.J., and Ewald, A.J. (2010). Morphogenesis of epithelial tubes: Insights into tube formation, elongation, and elaboration. Dev Biol *341*, 34-55.

Benton, M.A., Frey, N., Nunes da Fonseca, R., von Levetzow, C., Stappert, D., Hakeemi, M.S., Conrads, K.H., Pechmann, M., Panfilio, K.A., Lynch, J.A.*, et al.* (2019). Fog signaling has diverse roles in epithelial morphogenesis in insects. Elife *8*.

Benton, R., and St Johnston, D. (2003). Drosophila PAR-1 and 14-3-3 inhibit Bazooka/PAR-3 to establish complementary cortical domains in polarized cells. Cell *115*, 691-704.

Booth, A.J.R., Blanchard, G.B., Adams, R.J., and Roper, K. (2014). A dynamic microtubule cytoskeleton directs medial actomyosin function during tube formation. Dev Cell *29*, 562-576.

Cerniello, F.M., Carretero, O.A., Longo Carbajosa, N.A., Cerrato, B.D., Santos, R.A., Grecco, H.E., and Gironacci, M.M. (2017). MAS1 Receptor Trafficking Involves ERK1/2 Activation Through a beta-Arrestin2-Dependent Pathway. Hypertension *70*, 982-989.

Chung, S., and Andrew, D.J. (2014). Cadherin 99C regulates apical expansion and cell rearrangement during epithelial tube elongation. Development *141*, 1950-1960.

Chung, S., Hanlon, C.D., and Andrew, D.J. (2014). Building and specializing epithelial tubular organs: the Drosophila salivary gland as a model system for revealing how epithelial organs are specified, form and specialize. Wiley Interdiscip Rev Dev Biol *3*, 281-300.

Chung, S., Kim, S., and Andrew, D.J. (2017). Uncoupling apical constriction from tissue invagination. Elife *6*.

Dale, L.B., Seachrist, J.L., Babwah, A.V., and Ferguson, S.S. (2004). Regulation of angiotensin II type 1A receptor intracellular retention, degradation, and recycling by Rab5, Rab7, and Rab11 GTPases. J Biol Chem *279*, 13110-13118.

David, D.J., Tishkina, A., and Harris, T.J. (2010). The PAR complex regulates pulsed actomyosin contractions during amnioserosa apical constriction in Drosophila. Development *137*, 1645-1655.

Dunst, S., Kazimiers, T., von Zadow, F., Jambor, H., Sagner, A., Brankatschk, B., Mahmoud, A., Spannl, S., Tomancak, P., Eaton, S.*, et al.* (2015). Endogenously tagged rab proteins: a resource to study membrane trafficking in Drosophila. Dev Cell *33*, 351-365.

Fan, G.H., Lapierre, L.A., Goldenring, J.R., and Richmond, A. (2003). Differential regulation of CXCR2 trafficking by Rab GTPases. Blood *101*, 2115-2124.

Fuse, N., Yu, F., and Hirose, S. (2013). Gprk2 adjusts Fog signaling to organize cell movements in Drosophila gastrulation. Development *140*, 4246-4255.

842   Gorvel, J.P., Chavrier, P., Zerial, M., and Gruenberg, J. (1991). rab5 controls early
843   endosome fusion in vitro. Cell *64*, 915-925.
844   Gross, S.P., Welte, M.A., Block, S.M., and Wieschaus, E.F. (2000). Dynein-mediated
845   cargo transport in vivo. A switch controls travel distance. J Cell Biol *148*, 945-956.
846   Guglielmi, G., Barry, J.D., Huber, W., and De Renzis, S. (2015). An Optogenetic Method
847   to Modulate Cell Contractility during Tissue Morphogenesis. Dev Cell *35*, 646-660.
848   Hamelin, E., Theriault, C., Laroche, G., and Parent, J.L. (2005). The intracellular
849   trafficking of the G protein-coupled receptor TPbeta depends on a direct interaction with
850   Rab11. J Biol Chem *280*, 36195-36205.
851   Hunyady, L., Baukal, A.J., Gaborik, Z., Olivares-Reyes, J.A., Bor, M., Szaszak, M.,
852   Lodge, R., Catt, K.J., and Balla, T. (2002). Differential PI 3-kinase dependence of early
853   and late phases of recycling of the internalized AT1 angiotensin receptor. J Cell Biol
854   *157*, 1211-1222.
855   Innamorati, G., Le Gouill, C., Balamotis, M., and Birnbaumer, M. (2001). The long and
856   the short cycle. Alternative intracellular routes for trafficking of G-protein-coupled
857   receptors. J Biol Chem *276*, 13096-13103.
858   Izquierdo, E., Quinkler, T., and De Renzis, S. (2018). Guided morphogenesis through
859   optogenetic activation of Rho signalling during early Drosophila embryogenesis. Nat
860   Commun *9*, 2366.
861   Jouette, J., Guichet, A., and Claret, S.B. (2019). Dynein-mediated transport and
862   membrane trafficking control PAR3 polarised distribution. Elife *8*.
863   Kerridge, S., Munjal, A., Philippe, J.M., Jha, A., de las Bayonas, A.G., Saurin, A.J., and
864   Lecuit, T. (2016). Modular activation of Rho1 by GPCR signalling imparts polarized
865   myosin II activation during morphogenesis. Nat Cell Biol *18*, 261-270.
866   Khanal, I., Elbediwy, A., Diaz de la Loza Mdel, C., Fletcher, G.C., and Thompson, B.J.
867   (2016). Shot and Patronin polarise microtubules to direct membrane traffic and
868   biogenesis of microvilli in epithelia. J Cell Sci *129*, 2651-2659.
869   Ko, C.S., Tserunyan, V., and Martin, A.C. (2019). Microtubules promote intercellular
870   contractile force transmission during tissue folding. J Cell Biol *218*, 2726-2742.
871   Laan, L., Pavin, N., Husson, J., Romet-Lemonne, G., van Duijn, M., Lopez, M.P., Vale,
872   R.D., Julicher, F., Reck-Peterson, S.L., and Dogterom, M. (2012). Cortical dynein
873   controls microtubule dynamics to generate pulling forces that position microtubule
874   asters. Cell *148*, 502-514.
875   Langevin, J., Morgan, M.J., Sibarita, J.B., Aresta, S., Murthy, M., Schwarz, T., Camonis,
876   J., and Bellaiche, Y. (2005). Drosophila exocyst components Sec5, Sec6, and Sec15
877   regulate DE-Cadherin trafficking from recycling endosomes to the plasma membrane.
878   Dev Cell *9*, 365-376.
879   Le Droguen, P.M., Claret, S., Guichet, A., and Brodu, V. (2015). Microtubule-dependent
880   apical restriction of recycling endosomes sustains adherens junctions during
881   morphogenesis of the Drosophila tracheal system. Development *142*, 363-374.
882   Lee, J.Y., and Harland, R.M. (2010). Endocytosis is required for efficient apical
883   constriction during Xenopus gastrulation. Curr Biol *20*, 253-258.
884   Letizia, A., Sotillos, S., Campuzano, S., and Llimargas, M. (2011). Regulated Crb
885   accumulation controls apical constriction and invagination in Drosophila tracheal cells. J
886   Cell Sci *124*, 240-251.

887 Li, M., McGrail, M., Serr, M., and Hays, T.S. (1994). Drosophila cytoplasmic dynein, a
888 microtubule motor that is asymmetrically localized in the oocyte. J Cell Biol *126*, 1475-
889 1494.
890 Manning, A.J., Peters, K.A., Peifer, M., and Rogers, S.L. (2013). Regulation of epithelial
891 morphogenesis by the G protein-coupled receptor mist and its ligand fog. Sci Signal *6*,
892 ra98.
893 Manning, A.J., and Rogers, S.L. (2014). The Fog signaling pathway: insights into
894 signaling in morphogenesis. Dev Biol *394*, 6-14.
895 Martin, A.C., and Goldstein, B. (2014). Apical constriction: themes and variations on a
896 cellular mechanism driving morphogenesis. Development *141*, 1987-1998.
897 Martin, A.C., Kaschube, M., and Wieschaus, E.F. (2009). Pulsed contractions of an
898 actin-myosin network drive apical constriction. Nature *457*, 495-499.
899 Mason, F.M., Tworoger, M., and Martin, A.C. (2013). Apical domain polarization
900 localizes actin-myosin activity to drive ratchet-like apical constriction. Nat Cell Biol *15*,
901 926-936.
902 Meresse, S., Gorvel, J.P., and Chavrier, P. (1995). The rab7 GTPase resides on a
903 vesicular compartment connected to lysosomes. J Cell Sci *108 (Pt 11)*, 3349-3358.
904 Miao, H., Vanderleest, T.E., Jewett, C.E., Loerke, D., and Blankenship, J.T. (2019). Cell
905 ratcheting through the Sbf RabGEF directs force balancing and stepped apical
906 constriction. J Cell Biol.
907 Myat, M.M., and Andrew, D.J. (2000). Organ shape in the Drosophila salivary gland is
908 controlled by regulated, sequential internalization of the primordia. Development *127*,
909 679-691.
910 Myat, M.M., and Andrew, D.J. (2002). Epithelial tube morphology is determined by the
911 polarized growth and delivery of apical membrane. Cell *111*, 879-891.
912 Ossipova, O., Kim, K., Lake, B.B., Itoh, K., Ioannou, A., and Sokol, S.Y. (2014). Role of
913 Rab11 in planar cell polarity and apical constriction during vertebrate neural tube
914 closure. Nat Commun *5*, 3734.
915 Rauzi, M., Lenne, P.F., and Lecuit, T. (2010). Planar polarized actomyosin contractile
916 flows control epithelial junction remodelling. Nature *468*, 1110-1114.
917 Riggs, B., Rothwell, W., Mische, S., Hickson, G.R., Matheson, J., Hays, T.S., Gould,
918 G.W., and Sullivan, W. (2003). Actin cytoskeleton remodeling during early Drosophila
919 furrow formation requires recycling endosomal components Nuclear-fallout and Rab11.
920 J Cell Biol *163*, 143-154.
921 Roeth, J.F., Sawyer, J.K., Wilner, D.A., and Peifer, M. (2009). Rab11 helps maintain
922 apical crumbs and adherens junctions in the Drosophila embryonic ectoderm. PLoS
923 One *4*, e7634.
924 Roper, K. (2012). Anisotropy of Crumbs and aPKC drives myosin cable assembly
925 during tube formation. Dev Cell *23*, 939-953.
926 Royou, A., Field, C., Sisson, J.C., Sullivan, W., and Karess, R. (2004). Reassessing the
927 role and dynamics of nonmuscle myosin II during furrow formation in early Drosophila
928 embryos. Mol Biol Cell *15*, 838-850.
929 Sanchez-Corrales, Y.E., Blanchard, G.B., and Roper, K. (2018). Radially patterned cell
930 behaviours during tube budding from an epithelium. Elife *7*.

931 Sawyer, J.M., Harrell, J.R., Shemer, G., Sullivan-Brown, J., Roh-Johnson, M., and
932 Goldstein, B. (2010). Apical constriction: a cell shape change that can drive
933 morphogenesis. Dev Biol *341*, 5-19.
934 Sherwood, N.T., Sun, Q., Xue, M., Zhang, B., and Zinn, K. (2004). Drosophila spastin
935 regulates synaptic microtubule networks and is required for normal motor function.
936 PLoS Biol *2*, e429.
937 Sidor, C., Stevens, T.J., Jin, L., Boulanger, J., and Roper, K. (2020). Rho-Kinase Planar
938 Polarization at Tissue Boundaries Depends on Phospho-regulation of Membrane
939 Residence Time. Dev Cell *52*, 364-378 e367.
940 Ullrich, O., Reinsch, S., Urbe, S., Zerial, M., and Parton, R.G. (1996). Rab11 regulates
941 recycling through the pericentriolar recycling endosome. J Cell Biol *135*, 913-924.
942 Urbansky, S., Gonzalez Avalos, P., Wosch, M., and Lemke, S. (2016). Folded
943 gastrulation and T48 drive the evolution of coordinated mesoderm internalization in flies.
944 Elife *5*.
945 Volpicelli, L.A., Lah, J.J., Fang, G., Goldenring, J.R., and Levey, A.I. (2002). Rab11a
946 and myosin Vb regulate recycling of the M4 muscarinic acetylcholine receptor. J
947 Neurosci *22*, 9776-9784.
948 Westermann, S., and Weber, K. (2003). Post-translational modifications regulate
949 microtubule function. Nat Rev Mol Cell Biol *4*, 938-947.
950 Wichmann, H., Hengst, L., and Gallwitz, D. (1992). Endocytosis in yeast: evidence for
951 the involvement of a small GTP-binding protein (Ypt7p). Cell *71*, 1131-1142.
952 Wodarz, A., Grawe, F., and Knust, E. (1993). CRUMBS is involved in the control of
953 apical protein targeting during Drosophila epithelial development. Mech Dev *44*, 175-
954 187.
955 Yvon, A.M., Gross, D.J., and Wadsworth, P. (2001). Antagonistic forces generated by
956 myosin II and cytoplasmic dynein regulate microtubule turnover, movement, and
957 organization in interphase cells. Proc Natl Acad Sci U S A *98*, 8656-8661.
958 Zhang, X.M., Ellis, S., Sriratana, A., Mitchell, C.A., and Rowe, T. (2004). Sec15 is an
959 effector for the Rab11 GTPase in mammalian cells. J Biol Chem *279*, 43027-43034.

960